

**Repository of the Max Delbrück Center for Molecular Medicine (MDC)  
in the Helmholtz Association**

<https://edoc.mdc-berlin.de/17657>

**Structure and function of the global topsoil microbiome**

---

Bahram M., Hildebrand F., Forslund S.K., Anderson J.L., Soudzilovskaia N.A., Bodegom P.M., Bengtsson-Palme J., Anslan S., Coelho L.P., Harend H., Huerta-Cepas J., Medema M.H., Maltz M.R., Mundra S., Olsson P.A., Pent M., Põlme S., Sunagawa S., Ryberg M., Tedersoo L., Bork P.

This is the final version of the accepted manuscript. The original article has been published in final edited form in:

Nature  
2018 AUG 09 ; 560(7717): 233-237  
2018 AUG 01 (first published online: final version)  
doi: [10.1038/s41586-018-0386-6](https://doi.org/10.1038/s41586-018-0386-6)

Publisher: [Nature Research](#), part of Springer Nature

Publisher's notice

"This is a post-peer-review, pre-copyedit version of an article published in *Nature*. The final authenticated version is available online at: <https://dx.doi.org/10.1038/s41586-018-0386-6>".

# Structure and function of the global topsoil microbiome

Mohammad Bahram<sup>1,2,3\*</sup> †, Falk Hildebrand<sup>4\*</sup>, Sofía K. Forslund<sup>4,5,6</sup>, Jennifer L. Anderson<sup>2</sup>, Nadejda A. Soudzilovskaia<sup>7</sup>, Peter M. Bodegom<sup>7</sup>, Johan Bengtsson-Palme<sup>8,9</sup>, Sten Anslan<sup>1,10</sup>, Luis Pedro Coelho<sup>4</sup>, Helery Harend<sup>1</sup>, Jaime Huerta-Cepas<sup>4,11</sup>, Marnix H. Medema<sup>12</sup>, Mia R. Maltz<sup>13</sup>, Sunil Mundra<sup>14</sup>, Pål Axel Olsson<sup>15</sup>, Mari Pent<sup>1</sup>, Sergei Pölme<sup>1</sup>, Shinichi Sunagawa<sup>4,16</sup>, Martin Ryberg<sup>2</sup>, Leho Tedersoo<sup>17</sup> †, Peer Bork<sup>4,18,19</sup> †

<sup>1</sup>Department of Botany, Institute of Ecology and Earth Sciences, University of Tartu, 40 Lai St., 51005 Tartu, Estonia. <sup>2</sup>Department of Organismal Biology, Evolutionary Biology Centre, Uppsala University, Norbyvägen 18D, 75236 Uppsala, Sweden. <sup>3</sup>Department of Ecology, Swedish University of Agricultural Sciences, Ulls väg 16, 756 51 Uppsala, Sweden. <sup>4</sup>Structural and Computational Biology Unit, European Molecular Biology Laboratory, 69117 Heidelberg, Germany. <sup>5</sup>Current address: Experimental and Clinical Research Center, a cooperation of Charité-Universitätsmedizin Berlin and Max Delbrück Center for Molecular Medicine, 13125 Berlin, Germany. <sup>6</sup>Current address: Max Delbrück Centre for Molecular Medicine, 13125 Berlin, Germany. <sup>7</sup>Conservation Biology Department, Institute of Environmental Sciences, CML, Leiden University, Einsteinweg 2, 2333 CC Leiden, The Netherlands. <sup>8</sup>Department of Infectious Diseases, Institute of Biomedicine, The Sahlgrenska Academy, University of Gothenburg, Guldhedsgatan 10, SE-413 46 Göteborg, Sweden. <sup>9</sup>Centre for Antibiotic Resistance research (CARE) at University of Gothenburg, Göteborg, Sweden. <sup>10</sup>Braunschweig University of Technology, Zoological Institute, Mendelssohnstr. 4, 38106 Braunschweig, Germany. <sup>11</sup>Current address: Centro de Biotecnología y Genómica de Plantas, Universidad Politécnica de Madrid (UPM) - Instituto Nacional de Investigación y Tecnología Agraria y Alimentaria (INIA), Campus de Montegancedo-UPM, 28223-Pozuelo de Alarcón (Madrid) Spain. <sup>12</sup>Bioinformatics Group, Wageningen University, Droevendaalsesteeg 1, Wageningen, The Netherlands. <sup>13</sup>Center for Conservation Biology, University of California Riverside, USA Germany. <sup>14</sup>Section for Genetics and Evolutionary Biology (Evogene), Department of Biosciences, University of Oslo, P.O. Box 1066 Blindern, 0316 Oslo, Norway. <sup>15</sup>Biodiversity Unit, Department of Biology, Ecology building, Lund University, SE-223 62 Lund, Sweden. <sup>16</sup>Current address: Department of Biology, Institute of Microbiology, ETH Zurich, 8092 Zurich, Switzerland. <sup>17</sup>Natural History Museum, University of Tartu, 14A Ravila, 50411 Tartu, Estonia. <sup>18</sup>Max Delbrück Centre for Molecular Medicine, 13125 Berlin, Germany. <sup>19</sup>Department of Bioinformatics, University of Würzburg, 97074 Würzburg, Germany.

\*: These authors contributed equally.

†: Corresponding author.

## Summary

**Soils harbour some of Earth's most diverse microbiomes and are essential for both nutrient cycling and carbon storage. To understand soil functioning, it is necessary to model the global distribution patterns, biotic and environmental associations of the diversity and structure of both bacterial and fungal communities, and their functional gene repertoires<sup>1-</sup>**

44 **4. By leveraging metagenomics and metabarcoding of global topsoil samples (189 sites, 7560**  
45 **subsamples), we show that bacterial, but not fungal, genetic diversity is highest in**  
46 **temperate habitats and that microbial gene composition varies more strongly with**  
47 **environmental variables than geographic distance. We demonstrate that fungi and bacteria**  
48 **show global niche differentiation associated with contrasting diversity responses to**  
49 **precipitation and soil pH. Furthermore, we provide evidence for strong bacterial-fungal**  
50 **antagonism, inferred from antibiotics resistance genes, in topsoil and ocean habitats,**  
51 **indicating a substantial role of biotic interactions in shaping microbial communities. Our**  
52 **results suggest that both competition and environmental filtering affect bacterial and**  
53 **fungal abundance, composition and their encoded gene functions, implying spatially**  
54 **different relative contributions of these microbes to global nutrient cycling.**

55  
56 Bacteria and fungi dominate terrestrial soil habitats in terms of biodiversity, biomass, and their  
57 influence over essential soil processes<sup>5</sup>. Specific roles of microbial communities in  
58 biogeochemical processes are reflected by their taxonomic composition, biotic interactions and  
59 gene- functional potential<sup>1-4</sup>. While microbial biogeography studies have focused largely on  
60 single taxonomic groups, and on how their diversity and composition respond to local abiotic  
61 soil factors (e.g. pH<sup>6,7</sup>), both global patterns and the impact of biotic interactions on microbial  
62 biogeography remain relatively unexplored. In addition to constraints imposed by environmental  
63 factors, biotic interactions may strongly influence bacterial communities. For example, to  
64 outcompete bacteria, many fungal taxa secrete substantial amounts of antimicrobial compounds<sup>8</sup>,  
65 which select for antibiotic resistant (AR) bacteria and effectively increase relative antibiotic  
66 resistance gene (ARG) abundance. Here we employed metagenomics and DNA metabarcoding  
67 (16S, 18S, ITS rRNA gene markers), soil chemistry and biomass assessments (phospholipid fatty  
68 acids analyses, PLFAs) to determine the relationships among genetic (functional potential),  
69 phylogenetic, and taxonomic diversity and abundance in response to biotic and abiotic factors in  
70 189 topsoil samples, covering all terrestrial regions and biomes of the world<sup>9</sup> (Extended Data  
71 Figure 1a; Supplementary Table 1). Altogether 58,000 topsoil subsamples were collected from  
72 0.25-ha plots from 1450 sites (40 subsamples per site), harbouring homogeneous vegetation that  
73 were minimally affected by humans. We minimized biases and shortcomings in sampling<sup>10</sup> as  
74 well as technical variation including batch effects<sup>11</sup> by using highly standardized-collection and

75 processing protocols. From the total collection, 189 representative sites were selected for this  
76 analysis. We validated our main findings in external datasets, including an independent soil  
77 dataset (145 topsoil samples; Supplementary Table 1) that followed the same sampling and  
78 sequencing protocol.

79  
80 Using metagenomics, we constructed a gene catalogue for soils, by combining our newly  
81 generated data with published soil metagenomes (n=859, Supplementary Table 1) and identified  
82 159,907,547 unique genes (or fragments thereof). Only 0.51% of these 160 million genes  
83 overlapped with those from published genomes and large gut<sup>12</sup> and ocean<sup>13</sup> gene catalogues that  
84 are much closer to saturation (Supplementary Table 2), indicating that the functional potential of  
85 soil microbiomes is enormously vast and undersampled. For functional analysis, we annotated  
86 genes and functional modules via Orthologous Groups (OGs) using the eggNOG database<sup>14</sup>. For  
87 each sample, we also constructed taxonomic profiles at the class and phylum levels for both  
88 bacteria and fungi from relative abundance of rRNA genes in metagenomic datasets (miTags<sup>15</sup>),  
89 complemented by operational taxonomic units (OTUs) based on clustering 18S rRNA and  
90 internal transcribed spacer (ITS)<sup>16</sup> genes for soil fungi and 16S rRNA genes for soil bacteria at  
91 97% similarity threshold (see Methods). In total, 34,522 16S-based bacterial, 2,086 18S-based  
92 and 33,476 ITS-based fungal OTUs were analysed in the context of geographic space and 16  
93 edaphic and climatic parameters determined for each sampling site (see Methods). Archaea were  
94 poorly represented in our metabarcoding (<1% of OTUs) and metagenomics data (<1% miTags)  
95 and hence are excluded from most analyses.

96  
97 We examined whether the latitudinal diversity gradient (LDG), a trend of increasing diversity  
98 from the poles to the tropics seen in many macroscopic organisms, especially plants<sup>17</sup>, applies to  
99 microbial global distribution patterns<sup>10</sup>. We found that contrary to the typical LDG, both  
100 taxonomic and gene functional diversity of bacteria peaked at mid-latitudes and declined towards  
101 the poles and the equator, as is also seen in the global ocean<sup>13</sup>, although the pattern was relatively  
102 weak for taxonomic diversity herein (Figure 1a, c; Extended Data Figure 1b,2). The deviation of  
103 several bacterial phyla (5 of 20) from the general trends may be explained by responses to  
104 edaphic and climate factors weakly related to latitude (Extended Data Figure 1b) or contrasting  
105 effects at lower taxonomic levels (Supplementary discussion). In contrast, the LDG does apply to

106 overall fungal taxonomic diversity, and to 3 of 5 fungal phyla when examined separately, but not  
107 to fungal functional diversity, which was lowest in temperate biomes and exhibited an inverse  
108 unimodal relationship with latitude (Figure 1b,d; Extended Data Figure 2c). The LDG was  
109 negligible for oceanic fungi ( $p > 0.05$ )<sup>13</sup>, possibly due to their lower dispersal limitation and  
110 paucity of plant associations. While fungal taxonomic diversity decreased poleward, the total  
111 fungal biomass (inferred from PLFA markers) and the fungi-to-bacteria biomass ratio increased  
112 poleward, partly due to decline of bacterial biomass decreased with latitude (Extended Data  
113 Figure 3a-c).

114  
115 We tested the extent to which deterministic processes (such as competition and environmental  
116 filtering; i.e. the niche theory) *versus* neutral processes (dispersal and drift; the neutral theory)  
117 explain distributions of fungal and bacterial taxa and functions<sup>18</sup>. In bacteria, environmental  
118 variation correlated strongly with taxonomic composition (partial Mantel test accounting for  
119 geographic distance between samples:  $r_{\text{Env|Geo}} = 0.729$ ,  $p = 0.001$ ) and moderately with gene  
120 functional composition ( $r_{\text{Env|Geo}} = 0.100$ ,  $p = 0.001$ ), whereas the overall effect of geographic  
121 distance among samples was negligible ( $p > 0.05$ ). The weak correlation between geographic and  
122 taxonomic as well as functional composition suggests that environmental variables are more  
123 important than dispersal capacity in determining global distributions of soil bacteria and their  
124 encoded functions, as suggested by Baas Becking<sup>19</sup> and observed for oceanic prokaryotes<sup>13</sup>.

125  
126 For fungi, both geographic distance and environmental parameters were correlated with  
127 taxonomic composition (ITS data:  $r_{\text{Geo|Env}} = 0.307$ ,  $p = 0.001$ ;  $r_{\text{Env|Geo}} = 0.208$ ,  $p = 0.001$ ; 18S data:  
128  $r_{\text{Geo|Env}} = 0.193$ ,  $p = 0.001$ ;  $r_{\text{Env|Geo}} = 0.333$ ,  $p = 0.001$ ). Environmental distance (but not geographic  
129 distance) correlated with composition of fungal functional genes ( $r_{\text{Env|Geo}} = 0.197$ ,  $p = 0.001$ ), as  
130 also observed for bacteria. The relatively weaker correlation of fungi with environmental  
131 variation is consistent with results from local scales<sup>7</sup>. Thus, at both global and local scales,  
132 different processes appear to underlie community assembly of fungi and bacteria.

133  
134 To more specifically investigate the association of environmental parameters with the  
135 distribution of taxa and gene functions on a global scale, we used multiple regression modelling  
136 (see Methods). We found that bacterial taxonomic diversity, composition, richness and biomass

137 as well as relative abundance of major bacterial phyla can be explained by soil pH and nutrient  
138 concentration, and to a lesser extent by climatic variables (Extended Data Figures 4,5;  
139 Supplementary Table 4). Bacterial community composition responded most strongly to soil pH,  
140 followed by climatic variables, particularly mean annual precipitation (MAP; Extended Data  
141 Figures 4,5). This predominant role of pH agrees with studies from local to continental scales<sup>6</sup>,  
142 and may be ascribed to the direct effect of pH or confounded variables such as concentration of  
143 calcium and other cations<sup>6</sup>. The relative abundance of genes encoding several metabolic and  
144 transport pathways were strongly increased with pH (Extended Data Figure 4c), suggesting that  
145 there may be greater metabolic demand for these functions for bacteria in high-nutrient and  
146 alkaline conditions.

147  
148 Compared to temperate biomes, tropical and boreal habitats contained more closely related taxa  
149 at the tip of phylogenetic trees, but from more distantly related clades (Extended Data Figure  
150 2d), indicating a deeper evolutionary niche specialization in bacteria<sup>20</sup>. Together with global  
151 biomass patterns (Extended Data Figure 2a), these results suggest that soil bacterial communities  
152 in the tropics and at high latitudes are subjected to stronger environmental filtering and include a  
153 relatively greater proportion of edaphic niche specialists, possibly rendering these communities  
154 more vulnerable to global change. In contrast, phylogenetic overdispersion in temperate bacterial  
155 communities, may result from greater competitive pressure<sup>20</sup> or nutrient availability as predicted  
156 by the niche theory<sup>21</sup>.

157  
158 In contrast to the strong association between bacterial taxonomic diversity and soil pH, diversity  
159 of bacterial gene functions was more strongly correlated with MAP (Extended Data Figure 5a-h).  
160 The steeper LDG in gene functions than in taxa (Figure 1a,c) may thus relate to the stronger  
161 association of specific metabolic functions to climate than to local soil conditions. While soil and  
162 climate variables exhibited comparable correlations with fungal taxa, soil carbon-to-nitrogen  
163 (C/N) ratio was the major predictor for fungal biomass and relative abundance and composition  
164 of gene functions (Extended Data Figures 3g,4b,d; Supplementary Table 4). We hypothesize that  
165 compared to bacteria, global distribution of fungi is more limited by resource availability due to  
166 specialization for the use of specific compounds as substrates and greater energy demand.

167

168 We interpret opposing biogeographic trends for bacteria and fungi as niche segregation, driven  
169 by differential responses of bacteria and fungi to environmental factors<sup>7</sup> and their direct  
170 competition. Gene functional diversity of both bacteria and fungi responded to MAP and soil pH,  
171 albeit in opposite directions (Extended Data Figure 5c,d,g,h; Supplementary Table 3). This may  
172 partly explain the observed inverse pattern of gene functional diversity across the latitudinal  
173 gradient, i.e. niche differentiation, between bacteria and fungi (Figure 1; Extended Data Figure  
174 2). While increasing precipitation seems to favour higher fungal diversity, it is associated with  
175 higher B/F biomass and abundance ratios (Extended Data Figure 3d,g; Extended Data Figure  
176 5f,h). The increasing proportion of fungi towards higher latitudes may be explained by  
177 competitive advantages perhaps due to a greater tolerance to nutrient and water limitation  
178 associated with potential long-distance transport by hyphae.

179  
180 A role of inter-kingdom biotic interactions in determining the distributions of functional diversity  
181 and biomass in fungi and bacteria has been suggested previously<sup>22</sup>. As competition for resources  
182 affect the biomass of fungi and bacteria<sup>22,23</sup>, we hypothesized that B/F biomass ratio is related to  
183 the prevalence of fungi and bacterial ARG capacity because of broader activities of fungi than  
184 bacteria in utilizing complex carbon substrates<sup>24</sup> as well as increased antibiotic production of  
185 fungi in high C/N environments<sup>25</sup>. Consistent with this hypothesis, we found that both fungal  
186 biomass and the B/F biomass ratio correlated with ARG relative abundance (Extended Data  
187 Figure 6) and that most fungal OG subcategories, particularly those involved in biosynthesis of  
188 antibiotic and reactive oxygen species, increased with soil C/N ratio (Supplementary Table 4;  
189 Supplementary results). We also found that ARG relative abundance in topsoil is more strongly  
190 related to fungal relative abundance ( $r=0.435$ ,  $p<10^{-9}$ ) and B/F abundance ratio ( $r=-0.445$ ,  $p<10^{-12}$ ;  
191 Figure 2b) than to bacterial relative abundance ( $r=0.232$ ,  $p=0.002$ , based on miTags), which is  
192 supported by our external validation dataset (fungal relative abundance  $r=0.637$ ,  $p<10^{-15}$ ; B/F  
193 abundance ratio  $r=-0.621$ ,  $p<10^{-15}$ ; bacterial relative abundance  $r=0.174$ ,  $p=0.036$ ). Also, topsoil  
194 ARG relative abundance was significantly negatively correlated with bacterial phylogenetic  
195 diversity and OTU richness based on 16S rRNA gene (Extended Data Figures 7a,c,8a), further  
196 supporting a role for biotic interactions in shaping microbial communities.

197  
198 We also tested possible direct and indirect relationships between ARGs and 16 environmental

199 predictors using structural equation modelling (SEM; Supplementary Table 5). The optimized  
200 model suggests that soil C/N ratio and moisture, rather than pH – the predominant driver of  
201 bacterial diversity (Extended Data Figure 3g, Supplementary results) – affect B/F abundance  
202 ratio that in turn affects ARG relative abundance at the global scale (Figure 2c). In line increased  
203 antibiotics production in high competition environments, soil C/N ratio was the best predictor for  
204 richness of fungal functional genes ( $r^2=0.331$ ,  $p<10^{-15}$ ; Supplementary Table 3) and bacterial  
205 CAZyme genes involved in degrading fungal carbohydrates ( $r=0.501$ ,  $p<10^{-12}$ ). ARG relative  
206 abundance was also strongly correlated with C/N ratio in the external validation dataset ( $r=0.505$ ,  
207  $p<10^{-10}$ ).

208  
209 While the concomitant increase in AR potential and relative abundance of bacteria (as potential  
210 ARG carriers) was expected, the strong correlation of fungal relative abundance with ARG  
211 relative abundance and in turn bacterial phylogenetic diversity may be explained by selection  
212 against bacteria that lack ARGs, such that bacteria surviving fungal antagonism are enriched for  
213 ARGs. Among all studied phyla, the relative abundance of Chloroflexi, Nitrospirae, and  
214 Gemmatimonadetes bacteria (based on miTags), taxa with relatively low genomic ARG content  
215 (Supplementary Table 6) were most strongly negatively correlated with ARG relative abundance  
216 (Figure 3a). In contrast, ARGs were strongly positively correlated with the relative abundance of  
217 Proteobacteria, which have the greatest average number of ARGs per genome<sup>26</sup> among bacteria  
218 (Supplementary Table 6), and the fungal phyla Ascomycota and Zygomycota *s.lat.* (including  
219 Zoopagomycota and Mucoromycota) in both the global soil and the external validation sets  
220 (Figure 3a,b; Extended Data Figure 9a,c; Supplementary Table 7). More specifically, ITS  
221 metabarcoding revealed increasing relative abundances of ARGs with numerous fungal OTUs  
222 (Supplementary Table 8), particularly those belonging to *Oidiodendron* (Myxotrichaceae,  
223 Ascomycota) and *Penicillium* (Aspergillaceae, Ascomycota), which are known antibiotic  
224 producers<sup>27,28</sup> (Supplementary Results). Among bacterial ARGs, the relative abundance of efflux  
225 pumps and beta-lactamases, which act specifically on fungal-derived antibiotics, were  
226 significantly correlated to the relative abundance of Ascomycota (Extended Data Figure 10a;  
227 Supplementary Table 7). Actinobacteria, encompassing antibiotics-producing *Streptomyces*, also  
228 significantly correlated to ARG diversity in topsoil (Supplementary Table 6). Together these  
229 results suggest that relationships between organismal and ARG abundances are likely the result



230 of selective and/or suppressive actions of antibiotics on bacteria.

231  
232 Consistent with our observations in topsoil, we found evidence for antagonism between fungi  
233 and bacteria in oceans by reanalysing ARG distribution in 139 water samples from the global  
234 Tara Oceans project<sup>13</sup> (see Methods; Supplementary Table 1; Extended Data Figure 8a): the  
235 fungi-like stramenopile class Oomycetes (water moulds) and the fungal phylum Chytridiomycota  
236 constituted the groups most strongly associated with bacterial ARG relative abundance (Figure  
237 3a,c, Extended Data Figures 9b,d,10b,d). Although there is little direct evidence that oomycetes  
238 produce antibiotics, their high antagonistic activity can trigger bacteria<sup>29</sup> and other organisms  
239 including fungi<sup>30</sup> to produce antibiotics (Supplementary Discussion). As in topsoil, bacterial  
240 phylogenetic diversity was significantly negatively correlated with ARG relative abundance in  
241 ocean samples (Extended Data Figure 7b,c). In addition, the ARG relative abundance declined  
242 with increasing distance from the nearest coast in ocean samples (Extended Data Figure 8b),  
243 which may reflect the effect of a decreasing nutrient gradient along distance from the coast on  
244 the pattern of bacteria and fungi abundance and in turn ARG abundance. The agreement of  
245 results from these disparate habitats suggests that competition for resources related to nutrient  
246 availability and climate factors drive a eukaryotic-bacterial antagonism in both terrestrial and  
247 oceanic ecosystems.

248  
249 Our results indicate that both environmental filtering and niche differentiation determine global  
250 soil microbial composition, with a minor role of dispersal limitation at this scale (for limitations,  
251 see Methods). In particular, global distribution of soil bacteria and fungi was most strongly  
252 associated with soil pH and precipitation, respectively. Our data further indicate that inter-  
253 kingdom antagonism, as reflected in the association of bacterial ARGs with fungal relative  
254 abundance, is also important in structuring microbial communities. Although further studies are  
255 needed to explicitly address the interplay of B/F abundance ratio and ARG abundance, our data  
256 suggest that environmental variables that impact B/F abundance ratio may have consequences for  
257 microbial interactions and favouring fungi- or bacteria-driven soil nutrient cycling. This  
258 unprecedented view of global patterns of microbial distributions implies that global climate  
259 change may differentially affect bacterial and fungal composition and their functional potential,  
260 because acidification, nitrogen pollution and shifts in precipitation all have contrasting effects on

261 topsoil bacterial and fungal abundance, diversity and functioning.

262  
263 **Acknowledgments** The authors thank Ingrid Liiv for technical and laboratory assistance;  
264 Sebastian Waszak for constructive comments on the manuscript; Yan P. Yuan and Anna Glazek  
265 for bioinformatics support; and Alexander Holm Viborg for help in retrieving the CAZY  
266 database. We also thank Vladimir Benes, Rajna Hercog and other members of the EMBL  
267 GeneCore (Heidelberg), who provided assistance and facilities for sequencing. This study was  
268 funded by the Estonian Research Council (grants PUT171, PUT1317, PUT1399, IUT20-30,  
269 MOBERC, KIK, RMK, ECOLCHANGE), the Swedish Research Council (VR grant 2017-  
270 05019), Royal Swedish Academy of Sciences, Helge Axson Johnsons Stiftelse, EU COST  
271 Action FP1305 Biolink (STSM grant), Netherlands Organization for Scientific research (vidi  
272 grant 016.161.318), EMBL European Union's Horizon 2020 Research and Innovation  
273 Programme (#686070; DD-DeDaF) and Marie Skłodowska-Curie (600375).

274  
275 **Author Contributions** Author Contributions M.B., L.T. and P.B. conceived the project. L.T.  
276 supervised DNA extraction and sequencing. M.B., F.H., S.F., J.L.A., M.R. and P.B. designed  
277 and supervised the data analyses. F.H. designed and performed bioinformatics analysis. N.A.S  
278 and P.A.O. performed biomass analysis. S.F., S.M., M.P., S.A., H.H., S.P., M.R.M., S.S., and  
279 L.T. contributed data. M.B., F.H., S.F., J.L.A., P.M.B., S.A., J.B.P., M.H.M., L.P.C. and J.H.C.  
280 performed the data analyses. M.B. wrote the first draft of the manuscript with significant input  
281 from F.H., S.F., J.L.A., L.T. and P.B. All authors contributed to data interpretation and editing of  
282 the paper.

283  
284 **Author Information** The authors declare no competing financial interests. Correspondence  
285 should be addressed to P.B. ([bork@embl.de](mailto:bork@embl.de)), L.T. ([leho.tedersoo@ut.ee](mailto:leho.tedersoo@ut.ee)) or M.B.  
286 ([bahram@ut.ee](mailto:bahram@ut.ee)). Requests for materials should be addressed to M.B. ([bahram@ut.ee](mailto:bahram@ut.ee)) and F.H.  
287 ([falk.hildebrand@embl.de](mailto:falk.hildebrand@embl.de)).

288

289

## 290 **References**

291

- 292 1 Green, J. L., Bohannan, B. J. & Whitaker, R. J. Microbial biogeography: from taxonomy  
293 to traits. *Science* **320**, 1039-1043 (2008).
- 294 2 Reed, D. C., Algar, C. K., Huber, J. A. & Dick, G. J. Gene-centric approach to integrating  
295 environmental genomics and biogeochemical models. *Proc. Natl. Acad. Sci. USA* **111**,  
296 1879-1884 (2014).
- 297 3 Maynard, D. S., Crowther, T. W. & Bradford, M. A. Fungal interactions reduce carbon  
298 use efficiency. *Ecol. Lett.* **20**, 1034-1042 (2017).
- 299 4 de Menezes, A. B., Richardson, A. E. & Thrall, P. H. Linking fungal–bacterial co-  
300 occurrences to soil ecosystem function. *Curr. Opin. Microbiol.* **37**, 135-141 (2017).
- 301 5 Bardgett, R. D. & van der Putten, W. H. Belowground biodiversity and ecosystem  
302 functioning. *Nature* **515**, 505-511 (2014).
- 303 6 Lauber, C. L., Hamady, M., Knight, R. & Fierer, N. Pyrosequencing-based assessment of  
304 soil pH as a predictor of soil bacterial community structure at the continental scale. *Appl.*  
305 *Environ. Microbiol.* **75**, 5111-5120 (2009).

306 7 Rousk, J. *et al.* Soil bacterial and fungal communities across a pH gradient in an arable  
307 soil. *ISME J.* **4**, 1340 (2010).

308 8 de Boer, W., Folman, L. B., Summerbell, R. C. & Boddy, L. Living in a fungal world:  
309 impact of fungi on soil bacterial niche development. *FEMS Microbiol. Rev.* **29**, 795-811  
310 (2005).

311 9 Olson, D. M. *et al.* Terrestrial Ecoregions of the World: A New Map of Life on Earth: A  
312 new global map of terrestrial ecoregions provides an innovative tool for conserving  
313 biodiversity. *Bioscience* **51**, 933-938 (2001).

314 10 Green, J. & Bohannan, B. J. Spatial scaling of microbial biodiversity. *Trends Ecol. Evol.*  
315 **21**, 501-507 (2006).

316 11 Yuan, S., Cohen, D. B., Ravel, J., Abdo, Z. & Forney, L. J. Evaluation of methods for the  
317 extraction and purification of DNA from the human microbiome. *PLoS ONE* **7**, e33865  
318 (2012).

319 12 Li, J. *et al.* An integrated catalog of reference genes in the human gut microbiome. *Nat.*  
320 *Biotechnol.* **32**, 834-841 (2014).

321 13 Sunagawa, S. *et al.* Structure and function of the global ocean microbiome. *Science* **348**,  
322 1261359 (2015).

323 14 Huerta-Cepas, J. *et al.* eggNOG 4.5: a hierarchical orthology framework with improved  
324 functional annotations for eukaryotic, prokaryotic and viral sequences. *Nucleic Acids Res.*  
325 **44**, D286-D293 (2015).

326 15 Logares, R. *et al.* Metagenomic 16S rDNA Illumina tags are a powerful alternative to  
327 amplicon sequencing to explore diversity and structure of microbial communities.  
328 *Environ. Microbiol.* **16**, 2659-2671 (2014).

329 16 Tedersoo, L. *et al.* Global diversity and geography of soil fungi. *Science* **346**, 1078-+  
330 (2014).

331 17 Willig, M. R., Kaufman, D. & Stevens, R. Latitudinal gradients of biodiversity: pattern,  
332 process, scale, and synthesis. *Annu. Rev. Ecol. Syst.* **34**, 273-309 (2003).

333 18 Martiny, J. B. H. *et al.* Microbial biogeography: putting microorganisms on the map. *Nat.*  
334 *Rev. Microbiol.* **4**, 102-112 (2006).

335 19 Baas-Becking, L. G. M. *Geobiologie; of inleiding tot de milieukunde.* (WP Van Stockum  
336 & Zoon NV, 1934).

337 20 Webb, C. O., Ackerly, D. D., McPeck, M. A. & Donoghue, M. J. Phylogenies and  
338 community ecology. *Annu. Rev. Ecol. Syst.* **33**, 475-505 (2002).

339 21 Bryant, J. A., Stewart, F. J., Eppley, J. M. & DeLong, E. F. Microbial community  
340 phylogenetic and trait diversity declines with depth in a marine oxygen minimum zone.  
341 *Ecology* **93**, 1659-1673 (2012).

342 22 Frey-Klett, P. *et al.* Bacterial-fungal interactions: hyphens between agricultural, clinical,  
343 environmental, and food microbiologists. *Microbiol. Mol. Biol. Rev.* **75**, 583-609 (2011).

344 23 Mille-Lindblom, C., Fischer, H. & J Tranvik, L. Antagonism between bacteria and  
345 fungi: substrate competition and a possible tradeoff between fungal growth and tolerance  
346 towards bacteria. *Oikos* **113**, 233-242 (2006).

347 24 Koranda, M. *et al.* Fungal and bacterial utilization of organic substrates depends on  
348 substrate complexity and N availability. *FEMS Microbiol. Ecol.* **87**, 142-152 (2014).

349 25 Platas, G., Pelaez, F., Collado, J., Villuendas, G. & Diez, M. Screening of antimicrobial  
350 activities by aquatic hyphomycetes cultivated on various nutrient sources. *Cryptogamie:*  
351 *Mycol.* **19**, 33-43 (1998).

- 352 26 Mende, D. R. *et al.* proGenomes: a resource for consistent functional and taxonomic  
 353 annotations of prokaryotic genomes. *Nucleic Acids Res.*, D529-D534 (2017).
- 354 27 Bérdy, J. Thoughts and facts about antibiotics: where we are now and where we are  
 355 heading. *J. Antibiot.* **65**, 385-395 (2012).
- 356 28 Andersen, N. R. & Rasmussen, P. The constitution of clerocidin a new antibiotic isolated  
 357 from *Oidiodendron truncatum*. *Tetrahedron Lett.* **25**, 465-468 (1984).
- 358 29 Zhao, Y., Qian, G., Chen, Y., Du, L. & Liu, F. Transcriptional and antagonistic responses  
 359 of biocontrol strain *Lysobacter enzymogenes* OH11 to the plant pathogenic oomycete  
 360 *Pythium aphanidermatum*. *Front. Microbiol.* **8**, 1025 (2017).
- 361 30 Takahashi, K. *et al.* Cladomarine, a new anti-saprolegniasis compound isolated from the  
 362 deep-sea fungus, *Penicillium coralligerum* YK-247. *J. Antibiot.* **70**, 911 (2017).

363  
 364

## 365 Figure Legends

366

367 **Figure 1 | Fungal and bacterial diversity exhibit contrasting patterns across the latitudinal**  
 368 **gradient.** Latitudinal distributions of bacterial (left columns) and fungal (right columns)  
 369 taxonomic (**a** and **b**; n=188 biologically independent samples) and gene functional (**c** and **d**;  
 370 n=189 biologically independent samples) diversity in the global soil samples. The order of  
 371 polynomial fit was chosen based on the corrected Akaike Information Criterion (AICc; see  
 372 Methods) of first and second order polynomial models (ANOVA: **a**: F= 34.28;  $p < 10^{-7}$ ; **b**:  
 373 F=3.84,  $p = 0.052$ ; **c**: F= 50.48,  $p < 10^{-10}$ ; **d**: F= 18.55,  $p = p < 10^{-4}$ ). Grey dashed and black solid  
 374 lines are the first and second order polynomial regression lines, respectively. Diversity was  
 375 measured using Inverse Simpson Index (these trends were robust to choice of index, see  
 376 Extended Data Figure 2b, c). The latitudinal distribution of the high-level biome (tropical,  
 377 temperate and boreal-arctic) is given at the top of **a**) and **b**).

378

379 **Figure 2 | Global relative abundance of antibiotic resistance genes (ARGs) can be explained**  
 380 **by a combination of biotic and abiotic factors.** **a**, Pairwise Spearman correlation matrix of  
 381 main biotic and abiotic determinants of ARG relative abundance. **b**, B/F abundance ratio  
 382 significantly correlated with ARG relative abundance on a global scale. **c**, Structural equation  
 383 modelling (SEM) of ARG relative abundance of soil (green) and ocean (blue) datasets  
 384 (explaining 44% and 51% of variation, respectively; Supplementary Table 5). The goodness of  
 385 fit was acceptable (Soil: RMSEA=0.00, PCLOSE=0.989, n=189 biologically independent  
 386 samples; Ocean: RMSEA=0.059, PCLOSE=0.302, n=139 biologically independent samples).  
 387 Abbreviations: C/N, carbon to nitrogen ratio; N, nitrates; Bacteria/Fungi (B/F), the ratio of  
 388 bacterial to fungal abundance/biomass; Bacterial richness, bacterial OTU (>97% similarity)  
 389 richness based on metabarcoding dataset; Abundance, relative abundance of miTags determined  
 390 as fungi or bacteria; Biomass (nmol/g), absolute biomass based on PLFA analysis; MAP: mean  
 391 annual precipitation; MAT: mean annual temperature; n.a.: not applicable; n.s.: not significant  
 392 ( $p > 0.05$ ,  $q > 0.1$ ).

393

394 **Figure 3 | Fungi are the main determinants of antibiotic resistance gene (ARG) relative**  
 395 **abundance in soils and oceans.** **a**, The association between ARG relative abundance and major  
 396 bacterial and fungal (incl. fungal-like protist) phyla in metagenomic samples from soil and  
 397 ocean. Outer circle colour corresponds to the Pearson correlation coefficient. Circle fill colour

398 corresponds to significance after adjustment for multiple testing (q-value), as indicated in the  
399 legend. **b-c**, Relationships (non-parametric correlations) between the relative abundances of most  
400 correlated fungal groups with ARGs in soil metagenomes from this study (**b**) and ocean  
401 metagenomes (**c**). For statistical details and significance, see Supplementary Table 8. Asterisks  
402 denote significance after Benjamini-Hochberg correction for multiple testing (\*,  $q < 0.1$ ). See also  
403 supplementary analysis and Supplementary Table 8 for analogous results as in (**a**) but at the class  
404 level and in other habitats besides soil and ocean including published non-forest and agricultural  
405 soil as well as human skin and gut samples.

406  
407

## 408 **METHODS**

### 409 **Soil sample preparation**

410 Composite soil samples from 1450 sites worldwide were collected using highly standardized  
411 protocols<sup>16</sup>. The sampling was conducted broadly across the most influential known  
412 environmental gradient – the latitude - taking advantage of a global “natural laboratory” to study  
413 the impact of climate on diversity across vegetation, biome and soil types and to enable testing  
414 the effects of environmental parameters, spatial distance, and biotic interactions in structuring  
415 microbial communities. We carefully selected representative sites for different vegetation types  
416 separated by spatial distances sufficient to minimize spatial autocorrelation and to cover most  
417 areas of the globe. Total DNA was extracted from 2.0 g of soil from each sample using the  
418 PowerMax Soil DNA Isolation kit (MoBio, Carlsbad, CA, USA). A subset of 189 high-quality  
419 DNA samples representing different ecoregions spanning multiple forest, grassland and tundra  
420 biomes (Supplementary Table 1) were chosen for prokaryote and eukaryote metabarcoding  
421 (ribosomal rRNA genes) and whole metagenome analysis. Samples from desert (n=8: G4010,  
422 G4034, S357, S359, S411, S414, S418 and S421) and mangrove (n=1: G4023) biomes yielded  
423 sufficient DNA for metabarcoding, but not for metagenomics sequencing, thus these samples  
424 were used for global mapping of taxonomic diversity but excluded from all comparisons between  
425 functional and taxonomic diversity. One sample (S017) contained no 16S sequences; thus,  
426 altogether 189 and 197 samples were used for metagenomics and metabarcoding analyses,  
427 respectively.

428

429 To determine the functional gene composition of each sample, 5 µg total soil DNA (300-400 bp  
430 fragments) was ligated to Illumina adaptors using the TruSeq Nano DNA HT Library Prep Kit  
431 (Illumina Inc., San Diego, CA, USA) and shotgun-sequenced in three runs of the Illumina HiSeq  
432 2500 platform (2 × 250 bp paired-end chemistry, rapid run mode)<sup>31</sup> in the Estonian Genomics  
433 Center (Tartu, Estonia). Taxonomic composition was estimated from the same DNA samples  
434 using ribosomal DNA metabarcoding for bacteria (16S V4 subregion) and eukaryotes (18S V9  
435 subregion). For amplification of prokaryotes and eukaryotes, universal prokaryote primers 515F  
436 and 806RB<sup>32</sup> (although this pair may discriminate against certain groups of Archaea and Bacteria  
437 such as Crenarchaeota/Thaumarchaeota (and SAR11, see ref. <sup>33</sup>) and eukaryote primers 1389f  
438 and 1510r<sup>34</sup> were used. While the resolution of 16s rRNA sequencing is limited to genus (and  
439 higher) -level assignments, it is currently a standard approach in profiling bacterial communities  
440 and thus enabled us at least to explore patterns at coarse phylogenetic resolution.

441

442 Each primer was tagged with a 10-12-base identifier barcode<sup>16</sup>. DNA samples were amplified  
443 using the following PCR conditions: 95 °C for 15 min, followed by 30 cycles of 95 °C for 30 s,

444 50 °C 45 s and 72 °C for 1 min with a final extension step at 72 °C for 10 min. The 25 µl PCR  
445 mix consisted of 16 µl sterilized H<sub>2</sub>O, 5 µl 5× HOT FIREPol Blend MasterMix (Solis Biodyne,  
446 Tartu, Estonia), 0.5 µl each primer (200nM) and 3 µl template DNA. PCR products from three  
447 technical replicates were pooled and their relative quantity was evaluated after electrophoresis on  
448 an agarose gel. DNA samples producing no visible band or an overly strong band were amplified  
449 using 35 and 25 cycles, respectively. The amplicons were purified (FavorPrep™ Gel/PCR  
450 Purification Kit; Favorgen), checked for quality (ND 1000 spectrophotometer; NanoDrop  
451 Technologies), and quantified (Qubit dsDNA HS Assay Kit; Life Technologies). Quality and  
452 concentration of 16S amplicon pools were verified using Bioanalyzer HS DNA Analysis Kit  
453 (Agilent) and Qubit 2.0 Fluorometer with dsDNA HS Assay Kit (Thermo Fisher Scientific),  
454 respectively. Sequencing was performed on an Illumina MiSeq at the EMBL GeneCore facility  
455 (Heidelberg, Germany) using a v2 500 cycle kit, adjusting the read length to 300 and 200 bp for  
456 read1 and read2, respectively. 18S amplicon pools were quality checked using Bioanalyzer HS  
457 DNA Analysis Kit (Agilent), quantified using Qubit 2.0 Fluorometer with dsDNA HS Assay Kit  
458 (Thermo Fisher Scientific) and sequenced on an Illumina HiSeq at Estonian Genomics Center  
459 (Tartu, Estonia). Sequences resulting from potential contamination and tag-switching were  
460 identified and discarded based on two negative and positive control samples per sequencing run.  
461

### 462 **Soil chemical analysis and biomass analysis**

463 All topsoil samples were subjected to chemical analysis of pH<sub>KCl</sub>, P<sub>total</sub>, K, Ca and Mg; the  
464 content of <sup>12</sup>C, <sup>13</sup>C, <sup>14</sup>N and <sup>15</sup>N were determined using an elemental analyzer (Eurovector,  
465 Milan, Italy) coupled with an isotope ratio mass spectrometer<sup>55</sup>.

466  
467 To calculate the absolute abundance of bacteria and fungi using an independent approach,  
468 bacterial and fungal biomass were estimated from Phospholipid Fatty Acids (PLFAs)<sup>35</sup> in nmol/g  
469 as follows. Lipids were extracted from 2 g freeze dried soil in a one-phase solution of  
470 chloroform, methanol and citrate buffer<sup>36</sup>. Chloroform and citrate buffer was added to split the  
471 collected extract into one lipophilic phase, and one hydrophilic phase. The lipid phase was  
472 collected and applied on a pre-packed silica column<sup>36</sup>. The lipids were separated into neutral  
473 lipids, intermediate lipids and polar lipids (containing the phospholipids) by subsequent elution  
474 with chloroform, acetone and methanol. The neutral and phospholipids were dried using a speed  
475 vac. Methyl nonadecanoic acid (Me19:0) was added as an internal standard. The lipids were  
476 subjected to a mild alkaline methanolysis, in which fatty acids were derivatised to fatty acid  
477 methyl esters (FAMES). The FAMES from neutral (NLFAs) and phospholipids (PLFAs) were  
478 dried, using speed vac, and then dissolved in hexane before analysis on a gas-chromatograph as  
479 described by ref.<sup>37</sup>. Fungal biomass was estimated as the concentration of PLFA 18:2ω6,9 and  
480 bacterial biomass from the sum of nine PLFAs (i15:0, i16:0, i17:0, a15:0, a17:0, cy17:0, cy19:0,  
481 10Me17:0 and 10Me18:0)<sup>36</sup>. The nomenclature of fatty acids follows Frostegård et al.<sup>37</sup>.

### 482 **Acquisition of metadata from public databases**

483  
484 Climate data including monthly temperature and precipitation were obtained from the  
485 WorldClim database (www.worldclim.org). In addition, estimates of soil carbon, moisture, pH,  
486 potential evapotranspiration (PET) and net primary productivity (NPP) at 30 arc minute  
487 resolution were obtained from the Atlas of the Biosphere (www.sage.wisc.edu/atlas/maps.php).  
488 Samples were categorized into 11 biomes<sup>9</sup>, with all grassland biomes being categorized as  
489 “grasslands”. Thus, the following biomes were considered and summarized to three global

490 levels: moist tropical forests, tropical montane forests and dry tropical forests, savannas as  
491 tropical; Mediterranean, grasslands and shrublands, southern temperate forests, coniferous  
492 temperate forests and deciduous temperate forests as temperate; and boreal forests and arctic  
493 tundra as boreal-arctic. The time from the last fire disturbance was estimated based on inquiry  
494 from local authorities or collaborators and evidence from the field.  
495

## 496 **Metagenome analysis**

497 Most soil microbes are uncultured, making their identification difficult. Metagenomics analysis  
498 has emerged as a way around this to capture both genetic and phylogenetic diversity. As such it  
499 can only directly reveal the potential for functions through determining and tracing gene family  
500 abundances (as opposed to realized protein activity), which may be involved in various  
501 functional pathways<sup>38</sup>, but we can safely assume a strong correspondence between gene  
502 functional potential and the resulting ecosystem functioning<sup>39</sup> or enzyme activities<sup>40</sup>.  
503

504 Reads obtained from the shotgun metagenome sequencing of topsoil samples were quality-  
505 filtered, if the estimated accumulated error exceeded 2.5 with a probability of  $\geq 0.01$ <sup>41</sup>, or  $>1$   
506 ambiguous position. Reads were trimmed if base quality dropped below 20 in a window of 15  
507 bases at the 3' end, or if the accumulated error exceeded 2 using the sdm read filtering  
508 software<sup>42</sup>. After this, all reads shorter than 70% of the maximum expected read length (250 bp  
509 unless noted otherwise for external datasets) were removed. This resulted in retention of  
510 894,017,558 out of 1,307,037,136 reads in total (Supplementary Table 1). We implemented a  
511 direct mapping approach to estimate the functional gene composition of each sample. First, the  
512 quality-filtered read pairs were merged using FLASH<sup>43</sup>. The merged and unmerged reads were  
513 mapped against functional reference sequence databases (see below) using DIAMOND 0.8.10 in  
514 blastx mode<sup>44</sup> using “-k 5 -e 1e-4 --sensitive” options. The mapping scores of two unmerged  
515 query reads that mapped to the same target were combined to avoid double counting. In this case,  
516 the hit scores were combined by selecting the lower of the two e-values and the sum of the bit  
517 scores from the two hits. The best hit for a given query was based on the highest bit score,  
518 longest alignment length and highest percent identity to the subject sequence. Finally, aligned  
519 reads were filtered to those, having an alignment %identity  $>50\%$  and matching with an e-value  
520  $<1e-9$  (see below for parameter choice).  
521

522 The functional databases to which metagenomic reads were mapped included gene categories  
523 related to ROS sources (peroxidases genes databases<sup>45,46</sup>, KEGG<sup>47</sup> (Kyoto Encyclopedia of  
524 Genes and Genomes) and CAZyme genes ([www.cazy.org](http://www.cazy.org), accessed 22.11.2015)<sup>48</sup>). To facilitate  
525 interpretation of the results, the relative abundance of CAZyme genes were summed based on the  
526 substrates for each gene family. Substrate utilization information for CAZyme families was  
527 obtained from ref.<sup>49,50</sup> as well as CAZypedia  
528 ([http://www.cazypedia.org/index.php?title=Carbohydrate-binding\\_modules&oldid=9411](http://www.cazypedia.org/index.php?title=Carbohydrate-binding_modules&oldid=9411)). Based  
529 on the KEGG Ortholog (KO) abundance matrices we calculated SEED functional module  
530 abundances. For functional annotations of metagenomic reads, we used *in silico* annotation based  
531 on a curated database of the orthologous gene family resource eggNOG 4.5<sup>14</sup>.  
532

533 For all databases that included taxonomic information (eggNOG, KEGG, CAZY), reads were  
534 mapped competitively against all kingdoms and assigned into prokaryotic and eukaryotic groups,  
535 based on the best bit score in the alignment and the taxonomic annotation provided with the

536 database at kingdom level. All functional abundance matrices were normalized by the total  
537 number of reads used for mapping in the statistical analysis, unless mentioned otherwise (e.g.  
538 rarefied in the case of diversity analysis, see below). This normalization better takes into account  
539 differences in library size as it has the advantage of including the fraction of unmapped (that is  
540 functionally unclassified) reads. Although there are limitations in using relative abundance of  
541 genes, our analysis shows, which potential functions are relatively more important. Without any  
542 normalisation, such analyses cannot be performed. It is currently difficult to test the absolute  
543 numbers, due to limitations to reliably quantify soil DNA resulting from differences in extraction  
544 efficiency and level of degradation.

545  
546 To identify ARGs in our metagenome samples, the merged and unmerged reads were mapped to  
547 a homology expansion (see ref. <sup>51</sup>) of the Antibiotic Resistance gene Data Base (ARDB). Only  
548 hits surpassing the minimum sequence identity values as listed in the ARDB for each family  
549 were taken further into account. While there exist newer ARG databases, only the ARDB  
550 presently have curated family inclusion thresholds that directly allow application to our topsoil  
551 dataset: as soil microbial diversity is so large, unlike for gut datasets, high-fidelity gene  
552 catalogue construction will not be possible until many more samples are available. Therefore,  
553 direct mapping of reads to the gene family databases becomes necessary for our analysis, in turn  
554 necessitating ARG inclusion thresholds that are well-defined also for single reads, not merely for  
555 full-length genes. Thus, the cut-offs curated for e.g. ResFams<sup>52</sup> or CARD<sup>53</sup> are inappropriate,  
556 since they are defined in the length-dependent bit score space. The ARDB cut-offs, however, are  
557 defined as sequence identities, thus in principle applicable also to shorter than full-length  
558 sequences. Because of these technical limitations, we used a soil gene catalogue to determine  
559 CARD based ARG abundance matrices (see further on).

560  
561 It is important to note that functional gene including ARG measurements represent relative  
562 proportions of different gene families, because the absolute amount of DNA differs among  
563 samples. This necessitates, as we have done, to choose statistical tests that do not assume  
564 absolute measurements, and centres analysis of this type on comparisons across the set of  
565 samples.

### 566 **miTag taxa abundance estimation**

567 We used a miTag approach<sup>15</sup> to determine bacterial and fungal community composition from  
568 metagenome sequence data. First, SortMeRNA<sup>54</sup> was used to extract and blast search rRNA  
569 genes against the SILVA LSU/SSU database. Reads approximately matching these databases  
570 with e-values  $<10^{-1}$  were further filtered with custom Perl and C++ scripts, using FLASH to  
571 attempt merging all matched read pairs. In case read pairs could not be merged, as happens if the  
572 overlap between them is too small, the reads were interleaved such that the second read pair was  
573 reverse complemented and then sequentially added to the first read. To fine-match candidate  
574 interleaved or merged reads to Silva LSU/SSU databases, lambda<sup>55</sup> was used. Using the lowest  
575 common ancestor (LCA) algorithm adapted from LotuS (version 1.462)<sup>42</sup>, we determined the  
576 identity of filtered reads based on lambda hits. This included a filtering step, where queries were  
577 only assigned to phyla and classes if they had at least 88% and 91% similarity to the best  
578 database hit, respectively. The taxon by sample matrices were normalized by the total number of  
579 reads per sample to minimize the effects of uneven sequencing depth. The average of SSU and  
580 LSU matrices was used for calculating the relative abundance of phyla/classes. The abundance of  
581



582 miTag sequences matching bacteria and fungi was used to determine B/F abundance ratio. While  
583 LSU/SSU assessments refer to number of fungal cells rather than number of discrete  
584 multicellular fungi, since this can apply to all samples equally, it is not systematically biased for  
585 comparing the trends of bacterial to fungal abundance across samples.

586

### 587 **External metagenomic datasets**

588 We validate and compare the global trends with those on a smaller scale, we used a regional  
589 scale dataset of 145 topsoil generated and processed using the same protocol as our global  
590 dataset (Supplementary Table 1).

591

592 In addition, to compare patterns of ARG diversity in soils and oceans on a global scale, we re-  
593 analysed the metagenomics datasets of the Tara Oceans<sup>13</sup>, including all size fractions  
594 (Supplementary Table 1). After quality filtering, 41,790,928,650 out of 43,076,016,494 reads  
595 were retained from the Tara Oceans dataset.

596

597 The quality-filtered reads from all datasets were mapped to the corresponding databases using  
598 Diamond, with the exception that no merging of read pairs was attempted, because the chances  
599 of finding overlapping reads were too low (with a read length of 100 bp and insert size of 300 bp  
600 (Tara Oceans). Sequences for SSU/LSU miTags were extracted from these metagenomics  
601 datasets as described above. ARG abundance matrices were also obtained from the Tara Oceans  
602 project based on the published gene catalogues annotated using a similar approach as in the  
603 current study.

604

### 605 **Gene catalogue construction**

606 To create a gene catalogue, we first searched for complete reference genes that matched to read  
607 pairs in our collection using bowtie2<sup>56</sup> with the options “--no-unal --end-to-end”. The resulting  
608 bam files were sorted and indexed using samtools 1.3.1<sup>57</sup> and the  
609 `jgi_summarize_bam_contig_depths` provided with MetaBat<sup>58</sup> was used to create a depth profile  
610 of genes from the reference databases that were covered with  $\geq 95\%$  nucleotide identity. This cut-  
611 off is commonly used in constructing gene catalogues<sup>13,59</sup> and chosen to delineate genes  
612 belonging to the same species. Using the coverage information, we extracted all genes that had at  
613 least 200bp with  $\geq 1\times$  coverage by reads from our topsoil metagenomes. The reference databases  
614 included an ocean microbial gene catalogue<sup>13</sup>, a gut microbial gene catalogue<sup>12</sup>, as well as all  
615 genes extracted from 25,038 published bacterial genomes<sup>26</sup>. Altogether 273,723 and 2,376 and  
616 8,642 genes from proGenomes, IGC and Tara database, respectively, could be matched to soil  
617 reads and were used in the gene catalogue.

618

619 The majority of genes in our catalogue were assembled from the topsoil samples presented here.  
620 To reduce the likelihood of chimeric reads, each sample was assembled separately using Spades  
621 3.7-0 (development version obtained from the authors)<sup>60</sup> in metagenomic mode with the  
622 parameters “--only-assembler -m 500 --meta -k 21,33,67,111,127”. Only `sdm`<sup>42</sup> filtered paired  
623 reads were used in the assembly, with the same read filtering parameters as described above.  
624 Resulting assemblies had an average N50 of 469 bases (total of all assemblies 21,538 MBp). The  
625 low N50 reflects difficulties in the assembly of soil metagenomes, most likely reflecting the vast  
626 microbial genetic diversity of these ecosystems. We further *de novo* assembled reads from two  
627 other deep sequencing soil<sup>61</sup> and sediment studies<sup>62</sup>, using the same procedure and parameters,

628 except that the Spades parameter “-k 21,33,67,77” was adjusted to a shorter read length.  
629 Furthermore, we included publicly available data from the European Nucleotide Archive (ENA).  
630 ENA was queried to identify all projects with publicly available metagenomes and whose  
631 metadata contained the keyword "soil". The initial set of hits was then manually curated to select  
632 relevant project/samples that were assembled as described above. Additionally, we integrated  
633 gene predictions from soil metagenomes downloaded from MG-RAST<sup>63</sup> (Supplementary Table  
634 1). Assembly was not attempted for these samples due to the absence of paired end reads, and  
635 relatively low read depth; rather, only long reads or assemblies directly uploaded to MG-RAST  
636 with  $\geq 400$ bp length were retained. Therefore, only scaffolds and long reads, with at least 400 bp  
637 length, were used for analysis. On these filtered sequences genes were *de novo* predicted using  
638 prodigal 2.6.1<sup>64</sup> in metagenomic mode. Finally, we merged the predicted genes from assemblies,  
639 long reads, gene catalogues and references genomes to construct a comprehensive soil gene  
640 catalogue.

641  
642 Thus, 53,294,555,100 reads were processed, of which 31,015,827,636 (58.20%) passed our  
643 stringent quality control. The initial gene set predicted on the soil assemblies and long reads was  
644 separated into 17,114,295 complete genes and 111,875,596 incomplete genes. A non-redundant  
645 gene catalogue was built by comparing all genes to each other. This operation was performed  
646 initially in amino-acid space using DIAMOND<sup>44</sup>. Subsequently, any reported hits were checked  
647 in nucleotide space. Any gene that covered at least 90% of another one (with at least 95%  
648 identity over the covered area) was considered to be a potential representative of it (genes are  
649 also potential representatives of themselves). The final set was chosen by greedily picking the  
650 genes which are representative of the highest number of input genes until all genes in the original  
651 input have at least one representative in the output. This resulted in a gene catalogue with a total  
652 of 159,907,547 non-redundant genes at 95% nucleotide identity cut-off. We mapped reads from  
653 our experiment on the gene catalogue with bwa<sup>65</sup>, requiring  $>45$  nt overlap and  $>95\%$  identity.  
654 The average mapping rate was  $26.2 \pm 7.4\%$ . Although the gene catalogue is an invaluable  
655 resource for future explorations of the soil microbiome, we decided to rely on using the direct  
656 mapping approach to gene functional composition, due to the low overall mapping rate. Further,  
657 using minimap2<sup>66</sup> to find genes at 95% similarity threshold, we compared the soil gene catalogue  
658 with the Tara Oceans gene catalogue<sup>13</sup>, human gut gene catalogue<sup>12</sup> and the proGenomes  
659 prokaryotic database<sup>26</sup>. The gene catalogue nucleotide and amino acid sequences and abundance  
660 matrix estimates from rtk<sup>67</sup> have been deposited at [http://vm-  
661 lux.embl.de/~hildebra/Soil\\_gene\\_cat/](http://vm-lux.embl.de/~hildebra/Soil_gene_cat/).

### 662 663 **CARD ARG abundance estimation**

664 CARD abundances in topsoil samples were estimated by annotating the soil gene catalogue using  
665 a DIAMOND search of the predicted amino acid sequences against the CARD database and  
666 filtering hits to the specified bit-score cut-offs in the CARD database. Based on the gene  
667 abundances in each sample, we estimated the abundance of different CARD categories per  
668 metagenomic sample. Despite qualitative similarities in overall trends of ARDB and CARD  
669 abundance matrices, CARD abundance estimation is limited by being based on the gene  
670 catalogue (only a  $26.2 \pm 7.4\%$  of all metagenomic reads could be mapped to the gene catalogue).

### 671 672 **Processing of metabarcoding sequence data**

673 The LotuS pipeline<sup>42</sup> was used for bacterial 16S rRNA amplicon sequence processing. Reads  
674 were demultiplexed with modified quality-filtering settings for MiSeq reads, increasing strictness  
675 to avoid false positive OTUs. These modified options were the requirement of correctly detected  
676 forward 16S primer, trimming of reads after an accumulated error of 1 and rejecting reads below  
677 28 average quality or, exceeding an estimated accumulated error  $>2.5$  with a probability of  
678  $\geq 0.01$ <sup>41</sup>. Further, we required each unique read (reads preclustered at 100% identity) to be  
679 present 8 or more times in at least one sample, 4 or more times in at least two samples, or three  
680 or more times in at least three samples. In total 27,883,607 read pairs were quality-filtered and  
681 clustered with uparse<sup>68</sup> at 97% identity. Chimeric OTUs were detected and removed based on  
682 both reference-based and *de novo* chimera checking algorithms, using the RDP reference  
683 database ([http://drive5.com/uchime/rdp\\_gold.fa](http://drive5.com/uchime/rdp_gold.fa)) in uchime<sup>68</sup>, resulting in 13,070,436 high-  
684 quality read pairs to generate and estimate the abundance of bacterial OTUs. The seed sequence  
685 for each OTU cluster was selected from all read pairs assigned to that OTU, selecting the read  
686 pair with the highest overall quality and closest to the OTU centroid. Selected OTU seed read  
687 pairs were merged with FLASH<sup>43</sup> and a taxonomic identity was assigned to each OTU by  
688 aligning full-length sequences with lambda<sup>55</sup> to the SILVA v123 database<sup>69</sup> and the LotuS least  
689 common ancestor (LCA) algorithm. This was performed using the following LotuS command  
690 line options: "-p miSeq -derepMin 8:1,4:2,3:3 -simBasedTaxo 2 -refDB SLV -thr 8". OTU  
691 abundances per sample were summed to class and phylum level per sample, according to their  
692 taxonomic classification, to obtain taxa abundance matrices. However, the choice of clustering  
693 method (e.g. Swarm) and identity threshold had little effect on retrieved OTU richness  
694 (comparison with 99% threshold:  $r=0.977$ ,  $p<10^{-15}$ ; comparison with Swarm clustering:  $r=0.979$   
695  $p<10^{-15}$ ).

696  
697 For eukaryotic 18S rRNA genes, we used the same options in LotuS, except that reads were  
698 rejected if they did not occur at least six times each in a minimum of two samples or at least four  
699 times each in a minimum of three samples. This was done to account for lower sequencing depth  
700 in 18S rRNA compared to 16S rRNA dataset. Further, the database to annotate fungal taxonomy  
701 was extended to include general annotations of SILVA and information from unicellular  
702 eukaryotes (PR2 database<sup>70</sup>). Of 7,462,813 reads, 2,890,093 passed quality filtering. The fungal  
703 ITS metabarcoding dataset<sup>16</sup> was downloaded and used in addition to 18S data in specific  
704 analyses, such as finding associated fungal OTUs with ARG relative abundance. The resulting  
705 taxon abundance matrix was further filtered to remove sequences of chloroplast origin for all  
706 three metabarcoding experiments.

707  
708 Full-length sequences representing OTUs were aligned using the SILVA reference alignment as  
709 a template in mothur<sup>71</sup>. A phylogenetic tree was constructed using FastTree2<sup>72</sup> with the  
710 maximum-likelihood method using default settings. This program uses the Jukes-Cantor models  
711 to correct for multiple substitutions.

### 712 713 **Parametrization and validation of metagenomics approach**

714 Although we used state-of-art molecular approaches, there are several potential limitations  
715 regarding our analyses related to the used technologies. All metagenomics and amplicon-based  
716 analysis are affected by taxonomic biases in sequence databases, while (PCR-free) miTag as well  
717 as amplicon sequencing are biased due to differential ribosomal gene copy number across  
718 taxonomic groups. Amplicon-based metabarcoding, specifically, is affected by both primer PCR

719 artefacts and PCR biases that may affect estimates of absolute organism abundance. These biases  
720 are inherent to all metagenomics and metabarcoding studies. However, all these biases affect  
721 different samples equally (same rRNA gene copy numbers, same PCR biases per species, same  
722 database bias per taxa) and thus we estimate that our results are robust to these methodological  
723 shortcomings. Shotgun-based metagenomics is affected by reference bias, in which human  
724 pathogens or Proteobacteria are overrepresented. The necessity for lenient thresholds becomes  
725 obvious from annotating phylogenetic profiles with MetaPhlAn2<sup>73</sup> using standard parameters:  
726 while we observed that most fungal phyla are present abundantly in our samples, MetaPhlAn2  
727 detected Ascomycota only in 2 out of 189 samples. In 48 out of 189 samples, no organism  
728 (bacteria/archaea/eukaryotes) was detected, and the most abundant phylum was Proteobacteria  
729 (55%). Since these results are clearly deviating from our miTag, 16S, 18S and ITS based  
730 analysis, specific database cut-off thresholds were required for this project.

731  
732 To optimize the analysis pipeline and identify suitable e-values for filtering blastx results, we  
733 used metagenomic simulations of four reference genomes where CAZy assignments in the CAZy  
734 database were available. Simulated reads were created as 250 bp paired reads with 400 bp insert  
735 at differing sequence abundances from the four reference genomes in each simulated  
736 metagenome, using iMessi<sup>74</sup>. For this simulated dataset, we used the pipeline described above to  
737 derive CAZy functional profiles. We found that querying short reads processed as above against  
738 databases results in the retrieval of most genes at relative abundances consistent with  
739 expectations based on the reference genomes at e-value  $< 1e^{-9}$  ( $r=0.95\pm 0.01$ ,  $p<0.001$ ). Further,  
740 we simulated 200 metagenomes from 18 bacterial genomes, five bacterial plasmids, one fungal  
741 mitochondrion and two fungal genomes at differing relative proportions in each of these  
742 simulated metagenomes (Supplementary Table 11). We subsequently simulated 1,000,000 reads  
743 of 250 bp and 400 bp insert size using iMessi, and mapped these against reference databases and  
744 retained hits that fulfilled the following arbitrary criteria (used in all subsequent analyses): e-  
745 value cut-off of  $e^{-9}$ , alignment length  $\geq 20$  amino acids, and similarity  $\geq 50\%$  amino acids to the  
746 target sequence. From these, we generated functional profiles and found a strong correlation of  
747 simulated to expected functional metagenomic composition based on mixed fungal and bacterial  
748 genomes ( $r=0.94\pm 0.05$ ,  $p<0.001$ ).

### 749 **Estimating fungal antibiotics production**

751 We also specifically screened for fungal gene clusters directly associated with antibiotic activity,  
752 based on a compiled database of MiBIG (Minimum Information about a Biosynthetic Gene  
753 cluster, <https://mibig.secondarymetabolites.org>) repository entries that describe gene clusters for  
754 which the products have been shown experimentally to display antimicrobial activities  
755 (Supplementary Table 12). To extend the range of genes that can be associated with the  
756 validated, antibiotics producing, MiBIG protein domains, we downloaded all published non-  
757 redundant fungal genomes deposited in JGI (Supplementary Table 13) as well as all non-  
758 redundant fungal genes deposited in NCBI. The set of MiBIG, and fungal derived genes was  
759 screened with custom HMMs for domains from secondary metabolite production (specifically  
760 these were dmat, AMP-binding, Condensation, PKS\_KS and Terpene synthesis domains). All  
761 identified domains were aligned together with the MiBIG domains using Clustal Omega<sup>75</sup> and a  
762 tree was constructed with FastTree2. Phylogenetic trees were rooted to midpoint and  
763 automatically scanned to identify highly supported clades (aLRT branch support  $\geq 0.99$ ) where  
764 antibiotic producing MiBIG domains were monophyletically grouped. The average nucleotide

765 identity within each such group was subsequently used as identity cut-off in the mapping step.  
766 All metagenomic reads were mapped with diamond in blastx mode to the newly created  
767 database, using before-mentioned sequence identity cut-offs and rejecting domains of reads that  
768 were mapping to bacterial NOGs.

769

## 770 **Statistical analyses**

### 771 **Data normalization and diversity estimates**

772 All statistical analyses were performed using specific packages in R (version 3.3.2) unless  
773 otherwise noted. Diversity parameters were estimated from OTU and functional gene matrices  
774 that were rarefied to an equal number per sample to reduce the effect of variation in sequencing  
775 depth using the function *rrarefy* in *vegan* (version 2.2.1)<sup>76</sup>. ARG matrices were normalized by  
776 the total number of merged and singleton reads. Total abundance of ARGs per sample was  
777 estimated by summing the abundance of all individual ARGs per sample. ARG diversity  
778 measures indicate the variety and their proportions produced.

779

780 From the rarefied matrices we calculated OTU, OG and CAZyme gene richness (function  
781 *specnumber*) and diversity (function *diversity*, based on the Inverse Simpson index). The latter  
782 measure accounts for both richness and evenness, and it gives more weight to abundant groups  
783 compared to Shannon Index. Our results were robust to choice of index, and the various diversity  
784 indices highly correlated in the present dataset (e.g. bacterial taxonomic diversities calculated  
785 using Inverse Simpson versus using Shannon diversity were highly correlated:  $r=0.888$ ,  $p<10^{-15}$ ;  
786 for a comparison of richness and diversity trends, see Extended Data Figure 2b,c). Since  
787 evenness and richness were highly correlated in all datasets, we report the results based on  
788 diversity index that represent both richness and evenness. The rarefaction process was repeated  
789 for calculating taxonomic and gene functional diversity and richness based on the average of 100  
790 rarefied datasets.

791

792 Phylogenetic diversity was calculated based on Faith's Phylogenetic Diversity (PD) metric in  
793 *Picante* package of R<sup>77</sup>. In addition, to assess phylogenetic clustering and overdispersion, Nearest  
794 Relative Index (NRI) and Nearest Taxon Index (NTI) were calculated in *Picante*. Although both  
795 measures are closely related, NRI is more sensitive to phylogenetic diversity at deep nodes,  
796 whereas NTI is more sensitive to phylogenetic clustering towards tips. A null model of shuffling  
797 taxon labels (100 times) was used to randomize phylogenetic relationships among OTUs.

798

### 799 **Correlating environmental parameters to taxa and functions**

800 To identify the main determinants of taxonomic and gene functional composition or diversity  
801 and relative abundance of phyla/classes, we used a series of statistical tests. We included all  
802 prominent environmental variables that we expected to have a significant effect on microbial  
803 diversity based on previous studies, and which were feasible to collect. These included soil pH,  
804 carbon and nutrient levels and factors that can affect these, such as fire, assuming soil as the  
805 major resource for microbial nutrition. We also included isotope ratios of nitrogen ( $\delta^{15}\text{N}$ ) and  
806 carbon ( $\delta^{13}\text{C}$ ) as these provide principal components for carbon and nitrogen cycling. To avoid  
807 overfitting and to ensure model simplicity, we excluded the variables that had no significant  
808 impact on fungal or bacterial diversity, such as altitude, age of vegetation, plant diversity and  
809 community (the first two PCA axes of Plant community variation at both genus and family level)

810 and basal areas of trees. Thus, for univariate regression modelling, 16 variables (Supplementary  
811 Table 14) were included.

812  
813 To understand, which factors explain the OG- and OTU-based community composition, variable  
814 selection was performed in the *Forward.sel* function of Packfor (version 0.0-8/r109)<sup>78</sup> according  
815 to the coefficient of determination (threshold,  $r^2=0.01$ ). All functional and taxonomic  
816 compositional matrices were transformed using Hellinger transformation prior to statistical  
817 analysis. Further, Mantel tests and partial Mantel tests were used to test the effects of  
818 geographical *vs.* environmental distances on OTU and OG compositional similarity as  
819 implemented in *vegan*. Mantel tests allow testing the correlation of two distance matrices,  
820 whereas partial Mantel tests are similar but also control for variation in a third distance matrix. In  
821 our analysis, we controlled for the effect of geographic distance while testing the correlation of  
822 environmental variation and functional or taxonomic composition variation. The importance of  
823 biome type in explaining functional gene and taxonomic composition was tested in  
824 Permutational Multivariate Analysis of Variance (PERMANOVA) using the *Adonis* function of  
825 *vegan* (using  $10^3$  permutation for calculating pseudo-F test statistic and its statistical  
826 significance). For constructing OG and OTU distance matrices, the Bray-Curtis dissimilarity was  
827 calculated between each pair of samples. Great-circle distance was used to calculate a geographic  
828 distance matrix between samples based on geographical coordinates. This test compares the  
829 intragroup distances to intergroup distances in a permutation scheme and from this assesses  
830 significance. PERMANOVA post-hoc p-values were corrected for multiple testing using the  
831 Benjamini–Hochberg correction. We visualized taxonomic (OTU) and functional (OG)  
832 composition of bacteria using global nonmetric multidimensional scaling (GNMDS) in *vegan*  
833 with the following options: two dimensions, initial configurations = 100, maximum iterations =  
834 200, and minimum stress improvement in each iteration =  $10^{-7}$ . The main environmental drivers  
835 of the relative abundance of major taxonomic groups and main functional categories were  
836 recovered by random forest (RF) analysis<sup>79</sup> using the R-package *randomForest* (version 4.6-10).

837  
838 To examine latitudinal gradients of diversity at phylum level (Figure 2), the diversity of OTUs  
839 assigned to each phylum was calculated based on Inverse Simpson index. Diversity values were  
840 modelled in response to environmental variables and predicted values were extracted, which  
841 were used in a clustering and bootstrapping analysis to depict the similarities of phyla  
842 environmental associations using *pvclust* (version 1.3-2)<sup>80</sup> with 1000 iterations. To model  
843 latitudinal gradients and environmental associations of diversity and biomass (Figure 1,  
844 Extended Data Figure 3), we compared the goodness of fit estimates between first and second  
845 order polynomial models based on the corrected Akaike information criterion (AICc) using  
846 analysis of variance (ANOVA). AICc reflects both goodness of fit and parsimony of the models.

847  
848 For univariate regression modelling of diversity and biomass measures, *ordinary least squares*  
849 (*OLS*) or *generalized least squares* (*GLS*) regression models were employed depending on the  
850 importance of the spatial component. The model variance structure (Gaussian, exponential,  
851 spherical and linear) was evaluated based on AICc. Following selection of variance structure,  
852 variables were combined in a set of models with specified variance structure (i.e. number of  
853 tested models:  $2^{\text{number of variables}}$ ). The resulting models were sorted according to AICc values to  
854 reveal the best model. Lists of the 5 best-fitting models for each response variable are given in  
855 Supplementary Table 4. Prior to model selection, all variables were evaluated for linearity,

856 normality, and multicollinearity (excluded if the variance inflation factor was  $>5$ ). The degree of  
857 polynomial functions (linear, quadratic, cubic) was chosen based on the lowest AIC values.  
858 Because of non-linear relationships with response variables, a quadratic term for pH was also  
859 included in the model selection procedure. The accuracy of the final models was evaluated using  
860 10-fold 'leave-one-out' cross-validation. For this, we used 1000 randomly sampled 90%-data  
861 subsets for model training and predicting the withheld data. To minimize biases due to the  
862 partitioning of the data and potential overfitting, the average of 1000 resulting determination  
863 coefficients are reported as cross-validated  $r^2$  ( $r^2_{cv}$ ) for each regression model.

864

### 865 **Correlating biotic interactions to taxa and functions**

866 To test the associations of biotic variables on ARG relative abundance, we used a sparse partial  
867 least squares (sPLS) analysis, which reduces dimensionality by projecting predictor variables  
868 onto latent components to identify the 16S/18S lineages (phyla/classes) and the ITS OTUs most  
869 strongly associated with ARG relative abundance, as implemented in the mixOmics (version 5.0-  
870 4)<sup>81</sup> package. ARG composition and taxonomic community matrices (miTags classes/phyla and  
871 ITS OTUs) were normalized by library size using Hellinger transformation. Significance of  
872 associations was examined by bootstrap tests of subsets of each dataset. We subsequently used  
873 partial least squares (PLS) analysis to predict ARG relative abundance based on significantly  
874 correlated lineages, which allows the dimensionality of multivariate data to be reduced into PLS  
875 components. Optimal numbers of PLS components for prediction of the relative ARG abundance  
876 were selected based on leave-one-out cross-validation. To confirm the results of PLS analysis,  
877 we further used a cross-validated LASSO model to simultaneously perform variable selection  
878 and model fitting, as implemented in glmnet (version 2.0-2)<sup>82</sup>. First the lambda shrinkage  
879 parameter was determined from a cross-validated lasso-penalized logistic regression classifier.  
880 Using this shrinkage parameter, a new logistic regression classifier was fit to the data to predict  
881 ARG relative abundance.

882

883 To further test direct and indirect effects of geographic and environmental variables on microbial  
884 distributions, we built SEM models in the AMOS software (SPSS, Chicago, IL) by including  
885 predictors of the best GLS model. In *a priori* models, all indirect and direct links between  
886 variables were established based on their pairwise correlations. We subsequently removed non-  
887 significant links and variables or created new links between error terms until a significant model  
888 fit was achieved. Goodness of fit was assessed based on Chi-square test to evaluate the  
889 difference between observed and estimated by model covariance matrices (non-significant value  
890 indicates that the model fits the observed data). We also used Root Mean Square Error of  
891 Approximation (RMSEA) and *PCLOSE* (p-value for test of close fit) to assess the discrepancy  
892 between the observed data and model per degree of freedom, which is less sensitive to sample  
893 size compared to chi-square test (RMSEA  $< 0.08$  and *PCLOSE*  $> 0.05$  show a good fit).  
894 Observed correlations between diversity and environmental values can serve as the first step  
895 towards understanding the structure and function of global topsoil microbiome; however, they  
896 are not proof of causations and mechanism. Despite the fact that we used SEM modelling to infer  
897 indirect links, we cannot preclude the possibility of other biotic or soil variables confounded with  
898 climate variables that we did not include in our models. Further laboratory experiments may  
899 enable to address causality of relationships reported in this study.

900

901 Differences between univariate variables such as taxonomic and functional richness were tested  
902 using a non-parametric Wilcoxon rank-sum test, with Benjamini-Hochberg multiple testing  
903 correction. Post-hoc statistical testing for significant differences between all combinations of two  
904 groups was conducted only for taxa with  $p < 0.2$  in the Kruskal-Wallis test. For this, wilcoxon  
905 rank-sum tests were calculated for all possible group combinations and corrected for multiple  
906 testing using Benjamini-Hochberg multiple testing correction.

907  
908 Geographic coordinates were plotted on a world map transformed to a Winkler2 projection,  
909 using the maptools (version 0.8-36) package<sup>83</sup>.

### 910 **Limitations of statistical modelling on a global scale**

911 Although we performed cross-validations to test the accuracy of most of our statistical models,  
912 predictions might be limited by the vast diversity in soil microbiomes. For example, strong local  
913 variation in soil pH may lead to deviation from general patterns, which is a common limitation in  
914 environmental sciences. Given the large spatial scale and strong environmental gradient in our  
915 sampling design, and long-term persistence of DNA in soil<sup>84</sup>, seasonal variation in soils is  
916 expected to have a minor impact<sup>85</sup> (in contrast to ocean). In addition, the vast majority of our  
917 samples were collected during growing season, further reducing possible seasonal biases. We  
918 nevertheless tested the effect of sampling month and seasons and found no significant effect of  
919 seasonality on diversity indices ( $P > 0.05$ ). We also compared the effect of seasons and years in a  
920 time series study in two of our sites, which revealed no seasonal effects on richness and  
921 composition (unpublished data). In particular, the relationship between bacterial phylogenetic  
922 diversity and pH, are strongly consistent with studies performed at the local to continental scales  
923 and within a single season<sup>6,7,86</sup>, which indicates the robustness of our results. Nonetheless,  
924 validation of the proposed models needs to be performed by other researchers with extended data  
925 or an independent dataset, particularly by including samples from under-sampled regions  
926 (Extended Data Figure 1a) and from different seasons (to account for seasonality). For example,  
927 there were some under-sampled regions in our dataset (e.g. North Asia) lowering precision of our  
928 models for those regions. Unfortunately, there are no published global datasets with comparable  
929 sampling protocols used that could be directly compared and used for model validation, and we  
930 encourage future studies that will make this possible.

931  
932  
933 **Data availability** All metagenomics and metabarcoding sequences have been deposited in the  
934 European Bioinformatics Institute-Sequence Read Archive database, under accession number  
935 PRJEB24121 (ERP105926): Estonian forest and grassland topsoil samples; PRJEB19856  
936 (ERP021922): 16S metabarcoding data of global soil samples; PRJEB19855 (ERP021921): 18S  
937 metabarcoding data of global soil samples; PRJEB18701 (ERP020652): Global analysis of soil  
938 microbiomes. The soil gene catalogue and dataset are available at [http://vm-  
939 lux.embl.de/~hildebra/Soil\\_gene\\_cat/](http://vm-lux.embl.de/~hildebra/Soil_gene_cat/). The Tara Oceans data are available at [http://ocean-  
940 microbiome.embl.de/companion.html](http://ocean-microbiome.embl.de/companion.html). All other data that support the findings of this study are  
941 available from the corresponding authors upon request.  
942  
943



944 **Code availability** The pipeline to process metabarcoding samples is available under  
945 <http://psbweb05.psb.ugent.be/lotus/>. The pipeline to process shotgun metagenomic samples is  
946 available under <https://github.com/hildebra/MATAFILER> and  
947 <https://github.com/hildebra/Rarefaction>.

- 948  
949
- 950 31 Tedersoo, L. *et al.* Shotgun metagenomes and multiple primer pair-barcode combinations  
951 of amplicons reveal biases in metabarcoding analyses of fungi. *MycKeys* **10**, 1-43  
952 (2015).
- 953 32 Caporaso, J. G. *et al.* Global patterns of 16S rRNA diversity at a depth of millions of  
954 sequences per sample. *Proc. Natl. Acad. Sci. USA* **108**, 4516-4522 (2011).
- 955 33 Walters, W. *et al.* Improved bacterial 16S rRNA gene (V4 and V4-5) and fungal internal  
956 transcribed spacer marker gene primers for microbial community surveys. *mSystems* **1**,  
957 e00009-00015 (2016).
- 958 34 Amaral-Zettler, L. A., McCliment, E. A., Ducklow, H. W. & Huse, S. M. A method for  
959 studying protistan diversity using massively parallel sequencing of V9 hypervariable  
960 regions of small-subunit ribosomal RNA genes. *PLoS ONE* **4**, e6372 (2009).
- 961 35 Frostegård, Å., Tunlid, A. & Bååth, E. Use and misuse of PLFA measurements in soils.  
962 *Soil Biol. Biochem.* **43**, 1621-1625 (2011).
- 963 36 van Aarle, I. M. & Olsson, P. A. Fungal lipid accumulation and development of mycelial  
964 structures by two arbuscular mycorrhizal fungi. *Appl. Environ. Microbiol.* **69**, 6762-6767  
965 (2003).
- 966 37 Frostegård, Å., Tunlid, A. & Bååth, E. Phospholipid fatty acid composition, biomass, and  
967 activity of microbial communities from two soil types experimentally exposed to  
968 different heavy metals. *Appl. Environ. Microbiol.* **59**, 3605-3617 (1993).
- 969 38 Prosser, J. I. Dispersing misconceptions and identifying opportunities for the use  
970 of 'omics' in soil microbial ecology. *Nat. Rev. Microbiol.* **13**, 439-446 (2015).
- 971 39 Salles, J. F., Le Roux, X. & Poly, F. Relating phylogenetic and functional diversity  
972 among denitrifiers and quantifying their capacity to predict community functioning.  
973 *Front. Microbiol.* **3** (2012).
- 974 40 Trivedi, P. *et al.* Microbial regulation of the soil carbon cycle: evidence from gene-  
975 enzyme relationships. *ISME J.* **10**, 2593-2604 (2016).
- 976 41 Puente-Sánchez, F., Aguirre, J. & Parro, V. A novel conceptual approach to read-filtering  
977 in high-throughput amplicon sequencing studies. *Nucleic Acids Res.* **44**, e40-e40 (2016).
- 978 42 Hildebrand, F., Tadeo, R., Voigt, A. Y., Bork, P. & Raes, J. LotuS: an efficient and user-  
979 friendly OTU processing pipeline. *Microbiome* **2**, 30 (2014).
- 980 43 Magoc, T. & Salzberg, S. L. FLASH: fast length adjustment of short reads to improve  
981 genome assemblies. *Bioinformatics* **27**, 2957-2963 (2011).
- 982 44 Buchfink, B., Xie, C. & Huson, D. H. Fast and sensitive protein alignment using  
983 DIAMOND. *Nat. Methods* **12**, 59-60 (2015).
- 984 45 Choi, J. *et al.* fPoxDB: fungal peroxidase database for comparative genomics. *BMC*  
985 *Microbiol.* **14**, 117 (2014).
- 986 46 Fawal, N. *et al.* PeroxiBase: a database for large-scale evolutionary analysis of  
987 peroxidases. *Nucleic Acids Res.* **41**, D441-D444 (2012).
- 988 47 Kanehisa, M. & Goto, S. KEGG: kyoto encyclopedia of genes and genomes. *Nucleic*  
989 *Acids Res.* **28**, 27-30 (2000).

990 48 Cantarel, B. L. *et al.* The Carbohydrate-Active EnZymes database (CAZy): an expert  
991 resource for glycogenomics. *Nucleic Acids Res.* **37**, D233-D238 (2009).

992 49 Cantarel, B. L., Lombard, V. & Henrissat, B. Complex carbohydrate utilization by the  
993 healthy human microbiome. *PLoS ONE* **7**, e28742 (2012).

994 50 Cardenas, E. *et al.* Forest harvesting reduces the soil metagenomic potential for biomass  
995 decomposition. *ISME J.* **9**, 2465-2476 (2015).

996 51 Forslund, K. *et al.* Country-specific antibiotic use practices impact the human gut  
997 resistome. *Genome Res.* **23**, 1163-1169 (2013).

998 52 Gibson, M. K., Forsberg, K. J. & Dantas, G. Improved annotation of antibiotic resistance  
999 determinants reveals microbial resistomes cluster by ecology. *ISME J.* **9**, 207-216 (2015).

1000 53 McArthur, A. G. *et al.* The comprehensive antibiotic resistance database. *Antimicrob.*  
1001 *Agents Chemother.* **57**, 3348-3357 (2013).

1002 54 Kopylova, E., Noé, L. & Touzet, H. SortMeRNA: fast and accurate filtering of ribosomal  
1003 RNAs in metatranscriptomic data. *Bioinformatics* **28**, 3211-3217 (2012).

1004 55 Hauswedell, H., Singer, J. & Reinert, K. Lambda: the local aligner for massive biological  
1005 data. *Bioinformatics* **30**, i349-i355 (2014).

1006 56 Langmead, B. & Salzberg, S. L. Fast gapped-read alignment with Bowtie 2. *Nat. Methods*  
1007 **9**, 357-359 (2012).

1008 57 Li, H. *et al.* The Sequence Alignment/Map format and SAMtools. *Bioinformatics* **25**,  
1009 2078-2079 (2009).

1010 58 Kang, D. D., Froula, J., Egan, R. & Wang, Z. MetaBAT, an efficient tool for accurately  
1011 reconstructing single genomes from complex microbial communities. *PeerJ* **3**, e1165  
1012 (2015).

1013 59 Qin, J. *et al.* A human gut microbial gene catalogue established by metagenomic  
1014 sequencing. *Nature* **464**, 59 (2010).

1015 60 Bankevich, A. *et al.* SPAdes: a new genome assembly algorithm and its applications to  
1016 single-cell sequencing. *J. Comput. Biol.* **19**, 455-477 (2012).

1017 61 Howe, A. C. *et al.* Tackling soil diversity with the assembly of large, complex  
1018 metagenomes. *Proc. Natl. Acad. Sci. USA* **111**, 4904-4909 (2014).

1019 62 Sharon, I. *et al.* Accurate, multi-kb reads resolve complex populations and detect rare  
1020 microorganisms. *Genome Res.* **25**, 534-543 (2015).

1021 63 Meyer, F. *et al.* The metagenomics RAST server—a public resource for the automatic  
1022 phylogenetic and functional analysis of metagenomes. *BMC Bioinformatics* **9**, 386  
1023 (2008).

1024 64 Hyatt, D. *et al.* Prodigal: prokaryotic gene recognition and translation initiation site  
1025 identification. *BMC Bioinformatics* **11**, 119 (2010).

1026 65 Li, H. & Durbin, R. Fast and accurate short read alignment with Burrows–Wheeler  
1027 transform. *Bioinformatics* **25**, 1754-1760 (2009).

1028 66 Li, H. Minimap2: fast pairwise alignment for long DNA sequences. *arXiv:1708.01492*  
1029 (2017).

1030 67 Saary, P., Forslund, K., Bork, P. & Hildebrand, F. RTK: efficient rarefaction analysis of  
1031 large datasets. *Bioinformatics* **33**, 2594-2595 (2017).

1032 68 Edgar, R. C. UPARSE: highly accurate OTU sequences from microbial amplicon reads.  
1033 *Nat. Methods* **10** (2013).

- 1034 69 Pruesse, E. *et al.* SILVA: a comprehensive online resource for quality checked and  
 1035 aligned ribosomal RNA sequence data compatible with ARB. *Nucleic Acids Res.* **35**  
 1036 (2007).
- 1037 70 Guillou, L. *et al.* The Protist Ribosomal Reference database (PR2): a catalog of  
 1038 unicellular eukaryote small sub-unit rRNA sequences with curated taxonomy. *Nucleic*  
 1039 *Acids Res.*, gks1160 (2012).
- 1040 71 Schloss, P. D. *et al.* Introducing mothur: Open-Source, Platform-Independent,  
 1041 Community-Supported Software for Describing and Comparing Microbial Communities.  
 1042 *Appl. Environ. Microbiol.* **75**, 7537-7541 (2009).
- 1043 72 Price, M. N., Dehal, P. S. & Arkin, A. P. FastTree 2—approximately maximum-  
 1044 likelihood trees for large alignments. *PLoS ONE* **5** (2010).
- 1045 73 Truong, D. T. *et al.* MetaPhlan2 for enhanced metagenomic taxonomic profiling. *Nat.*  
 1046 *Methods* **12**, 902 (2015).
- 1047 74 Mende, D. R. *et al.* Assessment of metagenomic assembly using simulated next  
 1048 generation sequencing data. *PLoS ONE* **7**, e31386 (2012).
- 1049 75 Sievers, F. *et al.* Fast, scalable generation of high-quality protein multiple sequence  
 1050 alignments using Clustal Omega. *Mol. Syst. Biol.* **7** (2011).
- 1051 76 Oksanen, J. *et al.* Vegan: community ecology package. *R Package* (2015).
- 1052 77 Faith, D. P. Conservation evaluation and phylogenetic diversity. *Biol. Conserv.* **61**  
 1053 (1992).
- 1054 78 Dray, S., Blanchet, F. & Legendre, P. packfor: Forward selection with permutation. *R*  
 1055 *Package* (2013).
- 1056 79 Breiman, L. Random forests. *Mach. learn.* **45**, 5-32 (2001).
- 1057 80 Suzuki, R. & Shimodaira, H. pvelust: hierarchical clustering with p-values via multiscale  
 1058 bootstrap resampling. *R Package* (2009).
- 1059 81 Lê Cao, K. *et al.* mixOmics: Omics Data Integration Project. *R Package* (2017).
- 1060 82 Friedman, J. & Hastie, T. glmnet: lasso and elastic-net regularized generalized linear  
 1061 models. *R Package* (2015).
- 1062 83 Bivand, R. *et al.* Maptools: Tools for reading and handling spatial objects. *R package*  
 1063 (2015).
- 1064 84 Carini, P. *et al.* Relic DNA is abundant in soil and obscures estimates of soil microbial  
 1065 diversity. *Nat. Microbiol.* **2**, 16242 (2016).
- 1066 85 Žifčáková, L., Větrovský, T., Howe, A. & Baldrian, P. Microbial activity in forest soil  
 1067 reflects the changes in ecosystem properties between summer and winter. *Environ.*  
 1068 *Microbiol.* **18**, 288-301 (2016).
- 1069 86 Fierer, N. & Jackson, R. B. The diversity and biogeography of soil bacterial  
 1070 communities. *Proc. Natl. Acad. Sci. USA* **103**, 626-631 (2006).

1071  
 1072  
 1073

## 1074 **Extended Data legends**

1075

1076 **Extended Data Figure 1 | Distribution of topsoil samples and diversity patterns of phyla. a,**  
 1077 A map of samples used for metagenomic and metabarcoding analysis. Colours indicate biomes  
 1078 as indicated in the legend. Desert samples were only used in metabarcoding analysis and were  
 1079 excluded in comparative analysis of functional and taxonomic patterns. Black symbols refer to

1080 samples from an independent soil dataset (145 topsoil samples; Supplementary Table 1) that  
1081 were used for validation our results. **b**, Scatterplots showing the relationship between the  
1082 diversity of major microbial phyla (classes for Proteobacteria) and environmental variables  
1083 across the global soil samples (n=197 biologically independent samples). Only regression lines  
1084 for significant relationships after Bonferroni correction are shown. Diversity was measured using  
1085 Hellinger-transformed matrices based on Inverse Simpson Index. Latitude: absolute latitude;  
1086 MAP: mean annual precipitation; MAT: mean annual temperature; C/N: carbon to nitrogen ratio.

1087  
1088 **Extended Data Figure 2 | Contrasting microbial structure and function in major terrestrial**  
1089 **biomes. a-d**, The average total biomass (n=152 biologically independent samples) as well as  
1090 richness, diversity and relative abundance (n=188 biologically independent samples) of fungi and  
1091 bacteria across samples categorized into major terrestrial biomes, including tropical (moist and  
1092 dry tropical forests and savannas), temperate (coniferous and deciduous forests, grasslands and  
1093 shrublands, and Mediterranean biomes) and boreal-arctic ecosystems: total biomass (**a**); richness  
1094 (**b**); diversity (**c**); phylogenetic structure including Nearest relative index (NRI) and Nearest  
1095 taxon index (NTI) (see Methods) (**d**). **e-i**, Relative abundance of major phyla (n=188 biologically  
1096 independent samples) and functional categories (n=189 biologically independent samples) across  
1097 biomes: bacterial phyla (classes for Proteobacteria) and archaea (**e**); fungal classes (**f**); functional  
1098 categories of bacteria (**g**); functional categories of fungi (**h**); bacterial KEGG metabolic pathways  
1099 (**i**). Biomass was measured based on phospholipid-derived fatty acids (PLFA) analysis (see  
1100 Methods). Different letters denote significant differences between groups (shown in the legend)  
1101 at the 0.05 probability level based on Kruskal–Wallis test corrected for multiple testing.  
1102 Additional details for these comparisons are presented in Supplementary Table 14. Taxonomic  
1103 and gene functional diversity indices were calculated based on Inverse Simpson Index. The  
1104 centre values and error bars represent mean and SD, respectively.

1105  
1106 **Extended Data Figure 3 | Significant decline of bacterial to fungal biomass ratio with**  
1107 **increasing latitude due to the joint effect of climate and soil fertility. a**, The second order  
1108 polynomial relationship of absolute latitude and the total biomass of bacteria (n=152 biologically  
1109 independent samples). **b**, The relationship of absolute latitude and the total biomass of fungi. **c**,  
1110 The relationship of absolute latitude and the ratio of bacterial to fungal (B/F) biomass. **d-f**, The  
1111 relationship of B/F biomass ratio and mean annual precipitation (MAP), mean annual  
1112 temperature (MAT) and carbon to nitrogen ratio (C/N), as the main correlated environmental  
1113 variables with B/F biomass ratio. Linear regression analysis (Pearson correlation) was used in **b-f**  
1114 (n=152 biologically independent samples). **g**, Pairwise Spearman correlation matrix of biotic and  
1115 abiotic variables in soil. **h**, Direct and indirect relationships and directionality between variables  
1116 determined from Best-fitting Structural Equation Model. Determination coefficients ( $R^2$ ) are  
1117 given for biomass and diversity factors (see Supplementary Table 5 for more details). Goodness  
1118 of fit (see Methods): bacteria, Chi square=15.37, df=11, P=0.166; RMSEA=0.041,  
1119 PCLOSE=0.573, n=189; fungi, Chi square=7.74, df=12, P=0.805; RMSEA=0.00,  
1120 PCLOSE=0.970, n=189). Biomass (nmol/g) was measured based on phospholipid-derived fatty  
1121 acids (PLFA) analysis. pH, soil pH representing soil pH and its quadratic term; Ca, calcium; Mg,  
1122 magnesium; P, phosphorous; K, potassium; C, carbon; N, nitrogen;  $d^{15}N$ , nitrogen stable isotope  
1123 signature;  $d^{13}C$ , carbon stable isotope signature; PET, potential of evapotranspiration; Fire, time  
1124 from the last fire disturbance; NPP, net primary productivity.

1125

1126 **Extended Data Figure 4 | Environment has stronger effect on bacterial taxa and functions**  
1127 **than those of fungi.** Correlation and best random forest model for major taxonomic (**a** and **b**;  
1128 n=188 biologically independent samples) and functional (**c** and **d**; n=189 biologically  
1129 independent samples) categories of bacteria (left column) and fungi (right column) in the global  
1130 soil samples (n=189 biologically independent samples). **a**, Relative abundance of major 16S-  
1131 based bacterial phyla (class for Proteobacteria). **b**, Relative abundance of ITS-based fungal  
1132 classes. **c-d**, Major orthologous genes (OG) categories of bacteria (**c**) and fungi (**d**). For variable  
1133 selection and estimating predictability, the random forest machine-learning algorithm was used.  
1134 Circle size represents the variable importance, i.e. decrease in the prediction accuracy (estimated  
1135 with out-of-bag cross-validation) as a result of permutation of a given variable. Colours represent  
1136 Spearman correlations. pH, soil pH; Ca, calcium; Mg, magnesium; P, phosphorous; K,  
1137 potassium; C, carbon; N, nitrogen; d<sup>15</sup>N, nitrogen stable isotope signature; d<sup>13</sup>C, carbon stable  
1138 isotope signature; C/N, carbon to nitrogen ratio; Latitude, absolute latitude; MAP, mean annual  
1139 precipitation; MAT, mean annual temperature; PET, potential of evapotranspiration; Fire, time  
1140 from the last fire disturbance.

1141  
1142 **Extended Data Figure 5 | Niche differentiation between bacteria and fungi is likely related**  
1143 **to precipitation and soil pH.** Contrasting effect of pH and mean annual precipitation (MAP) on  
1144 bacterial (16S; left columns) and fungal (18S; right columns) taxonomic (n=188 biologically  
1145 independent samples) and gene functional (n=189 biologically independent samples) diversity in  
1146 the global soil samples: **a, b**, Relationship of soil pH and taxonomic diversity of bacteria (**a**) and  
1147 fungi (**b**); **c, d**, Relationship of soil pH and gene functional diversity of bacteria (**c**) and fungi (**d**);  
1148 **e, f**, Relationship of MAP and taxonomic diversity of bacteria (**e**) and fungi (**f**); **g, h**,  
1149 Relationship of MAP and gene functional diversity of bacteria (**g**) and fungi (**h**). Lines represent  
1150 regression lines of best fit. The choice of degree of polynomial was determined by a goodness of  
1151 fit (see Methods). Colours denote biomes as indicated in the legend. MAP: mean annual  
1152 precipitation. Taxonomic and gene functional diversity indices were calculated based on Inverse  
1153 Simpson Index. **i-l**, Non-metric multidimensional scaling (NMDS) plots of trends in taxonomic  
1154 (16S and 18S-based datasets) and gene functional composition (OGs from metagenomes) of  
1155 bacteria (left column) and fungi (right column) based on Bray-Curtis dissimilarity. Taxonomic  
1156 composition of bacteria (16S). **j**, Taxonomic composition of fungi (18S). **k**, Gene functional  
1157 composition of bacteria. **l**, Gene functional composition of fungi. **i**, Colours denote biomes as  
1158 indicated in the legend. Vectors are the prominent environmental drivers fitted onto ordination.

1159  
1160 **Extended Data Figure 6 | Fungal biomass is significantly related to the relative abundance**  
1161 **of antibiotic resistance genes (ARG).** **a**, Increase in fungal biomass is related to ARG relative  
1162 abundance. **b**, Bacterial biomass is unrelated to ARG relative abundance. **c**, ARG relative  
1163 abundance is inversely correlated with Bacteria-to-Fungi biomass ratio. Biomass (nmol/g) was  
1164 measured based on Phospholipid Fatty Acids (PLFA) analysis (see Methods). Spearman  
1165 correlation was used (n=152 biologically independent samples).

1166  
1167 **Extended Data Figure 7 | Topsoil and ocean bacterial phylogenetic diversity is negatively**  
1168 **correlated with the abundance of antibiotic resistance genes.** **a, b**, Spearman correlations  
1169 between ARG relative abundance and bacterial phylogenetic diversity (Faith's index; see  
1170 Methods) in soil (n=188 biologically independent samples). (**a**) and ocean (n=139 biologically  
1171 independent samples). (**b**) at the global scale. Similar trends were observed for richness (r=-

1172 0.219,  $p=0.007$  and  $r=-0.659$ ,  $p<10^{-15}$ ) in soil and ocean, respectively). **c**, Global map of  
1173 observed bacterial phylogenetic diversity (Faith's index; see Methods) at the sampled sites. Note  
1174 that hotspots of bacterial diversity do not correspond to hotspots of ARG relative abundance (See  
1175 Extended Data Figure 8).

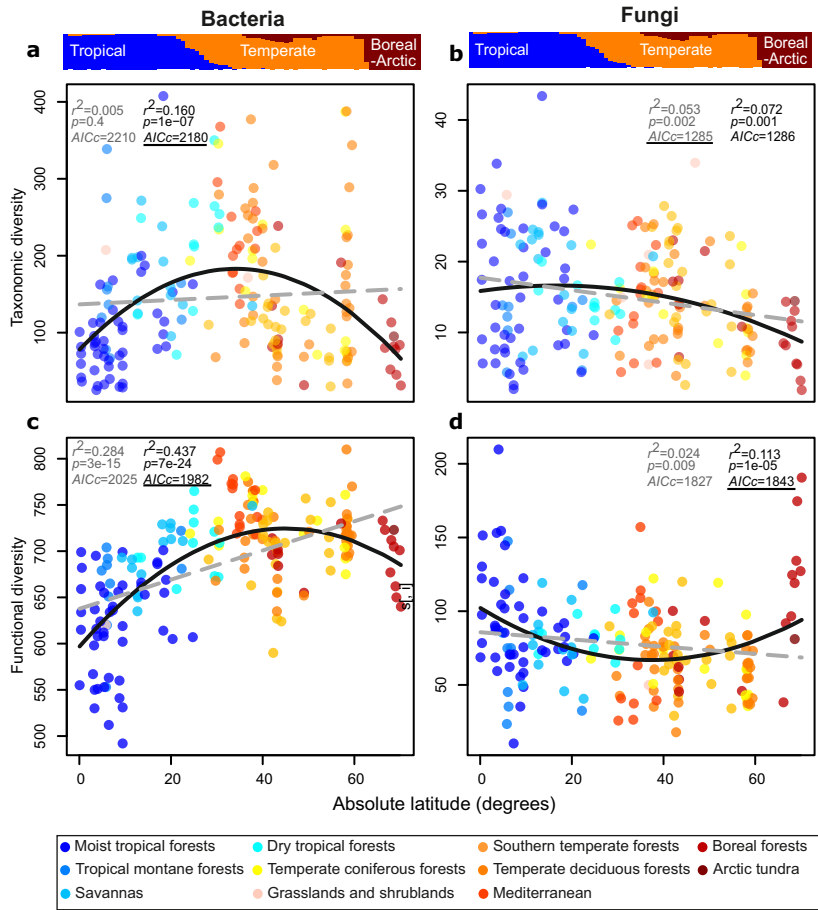
1176  
1177 **Extended Data Figure 8 | Antibiotic resistance gene (ARG) relative abundance within and**  
1178 **between terrestrial and oceanic ecosystems. a**, Heat map of observed antibiotic resistance gene  
1179 (ARG) relative abundance at the global scale. Squares and circles correspond to soil and to ocean  
1180 samples, respectively. ARG abundance is given on three relative scales for these three datasets.  
1181 **b**, ARG relative abundance in ocean samples (across depths) declines with distance from land  
1182 ( $n=139$  biologically independent samples), a pattern which was significant at two water depths,  
1183 including surface (red) and deep chlorophyll maximum (DCM; green), but not at mesopelagic  
1184 (blue). Spearman correlation statistics for specified comparisons are given in the legends. Dotted  
1185 lines display Spearman correlations across the whole dataset and within the three depth  
1186 categories, respectively.  $n$ : number of biologically independent samples.

1187  
1188 **Extended Data Figure 9 | Antibiotic resistance gene (ARG) relative abundance in both**  
1189 **ocean and topsoil samples can be modelled by the relative abundance of fungi and fungi-**  
1190 **like protists. a, b**, Correlation circle indicating the relationships among fungal classes and ARG  
1191 relative abundance as well as the first two partial least squares regression (PLS) components.  
1192 Length and direction of vectors indicate the strength and direction of correlations. Percentages  
1193 show the variation explained by each PLS component. **c, d**, Linear (Pearson) correlations  
1194 between observed and modelled ARG relative abundance based on the relative abundance of  
1195 fungal taxa in soil (**c**) and ocean (**d**). The two principal axes were chosen based on leave-one-out  
1196 cross-validation (LOOCV) and explained 42% (LOOCV:  $R^2=0.401$ ) and 71% (LOOCV:  
1197  $r^2=0.684$ ) of the variation of ARG relative abundance in soil and ocean, respectively. Only taxa  
1198 significantly associated with ARG relative abundance are shown. Cross validation and Lasso  
1199 regression confirmed this result: soil dataset:  $r=0.619$ ,  $RMSE=10^{-9}$ ;  $n=189$  biologically  
1200 independent samples; Ocean dataset,  $r=0.832$ ,  $RMSE=10^{-9}$ ;  $n=139$  biologically independent  
1201 samples.

1202  
1203 **Extended Data Figure 10 | Fungal classes are among the main taxa associated with**  
1204 **antibiotic resistance gene (ARG) relative abundance, diversity and richness in different**  
1205 **habitats. a, b**, Heat map derived from sPLS analysis showing correlation of total ARG relative  
1206 abundance, richness and diversity to that of the main taxonomic classes in soil (**a**) and ocean (**b**)  
1207 metagenomes (see also the supplementary results for analogous results in previously published  
1208 soil (from grasslands, deserts agricultural soils) as well as human skin and gut samples). For  
1209 statistical details and significance, see Supplementary Table 8. **c, d**, Heat maps showing  
1210 correlation of total ARG relative abundance to that of the main eukaryotic and prokaryotic taxa  
1211 in soil (**c**) and ocean (**d**) based on sparse partial least square (sPLS) regression analysis. All  
1212 matrices were normalized by library size and Hellinger transformation. Fungal and fungal-like  
1213 classes are shown in bold text. See Supplementary Table 15 for ARG gene letter abbreviations.

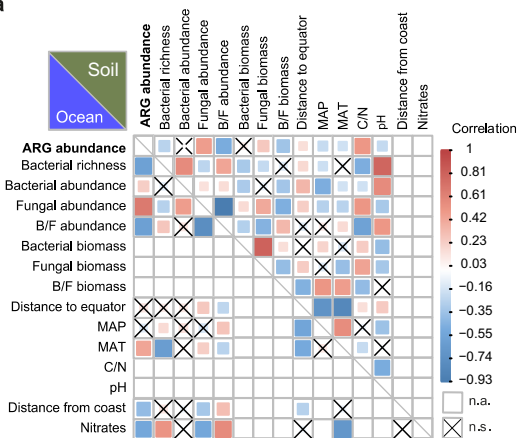
1214  
1215  
1216  
1217

Figure 1

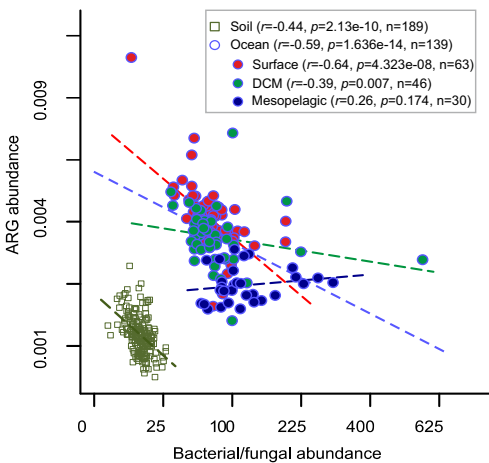


# Figure 2

**a**



**b**



**c**

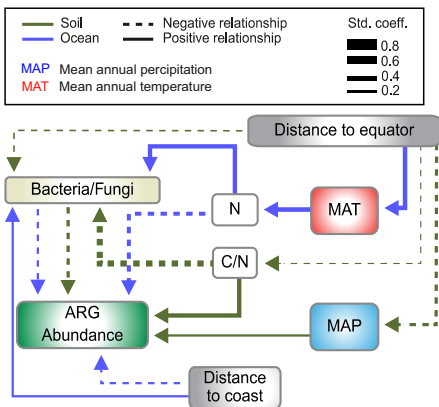
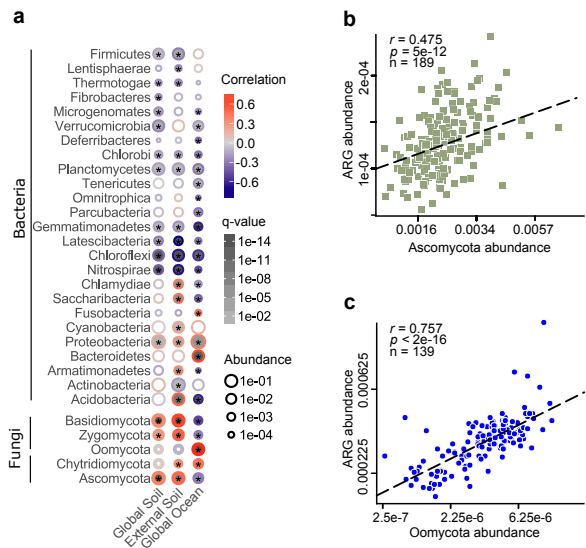


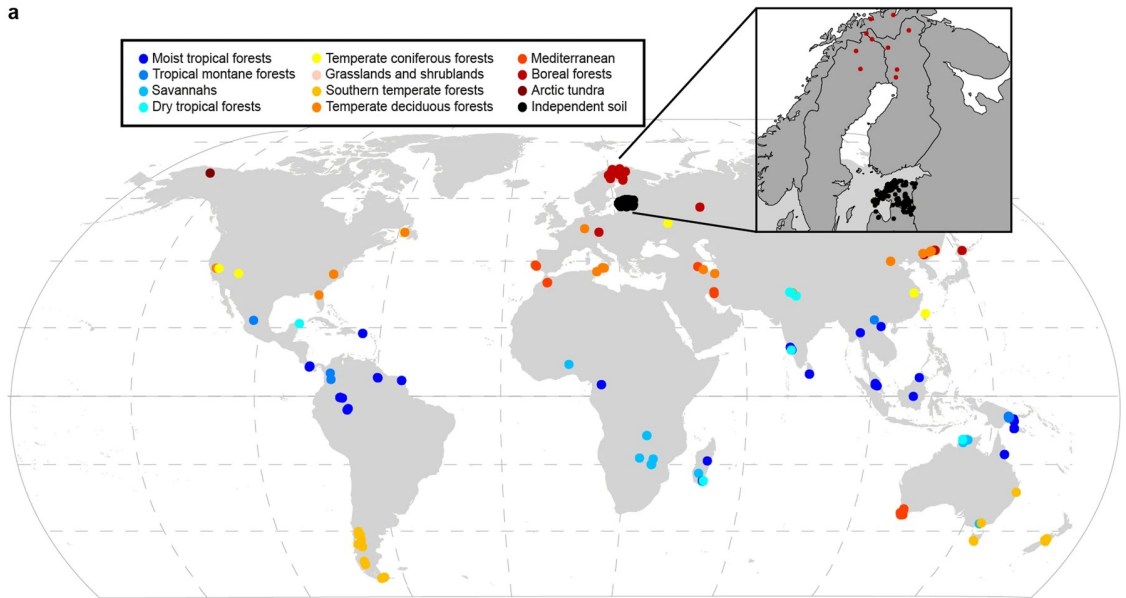


# Figure 3

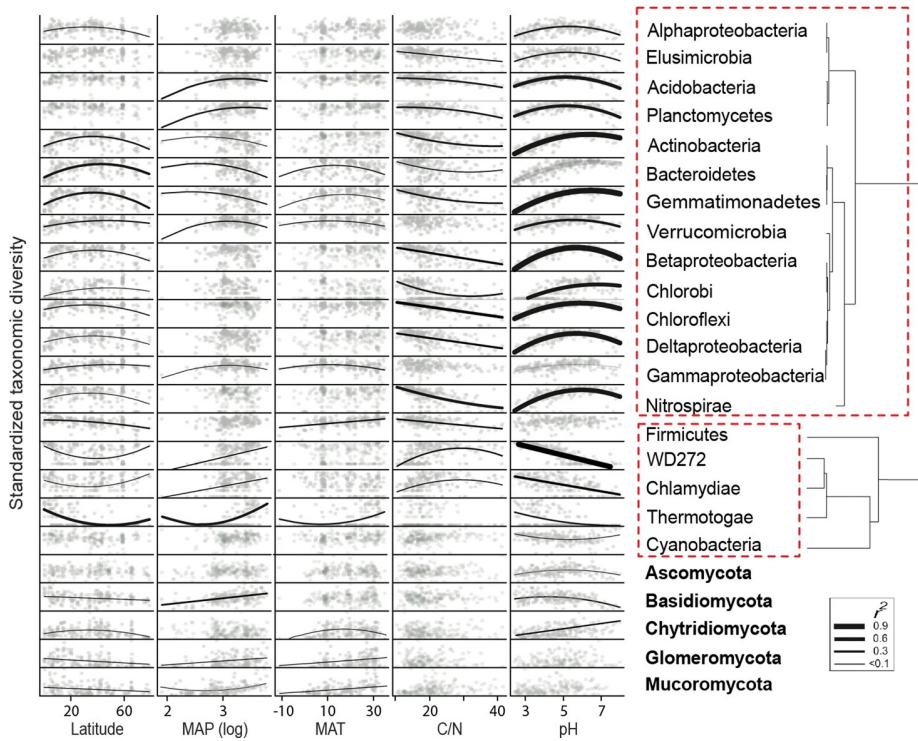


# Extended Data Fig. 1 Distribution of topsoil samples and diversity patterns of phyla.

a

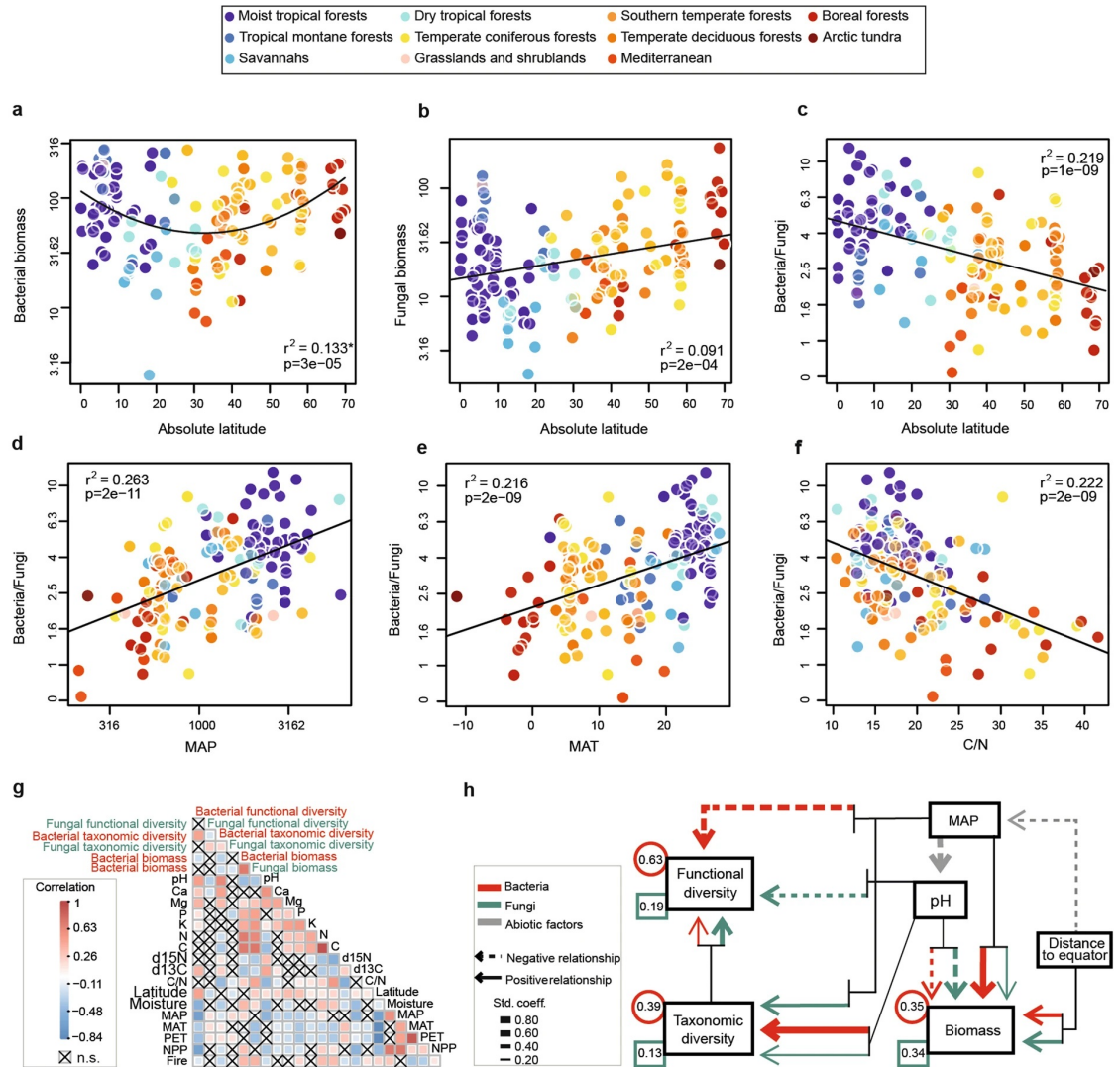


b

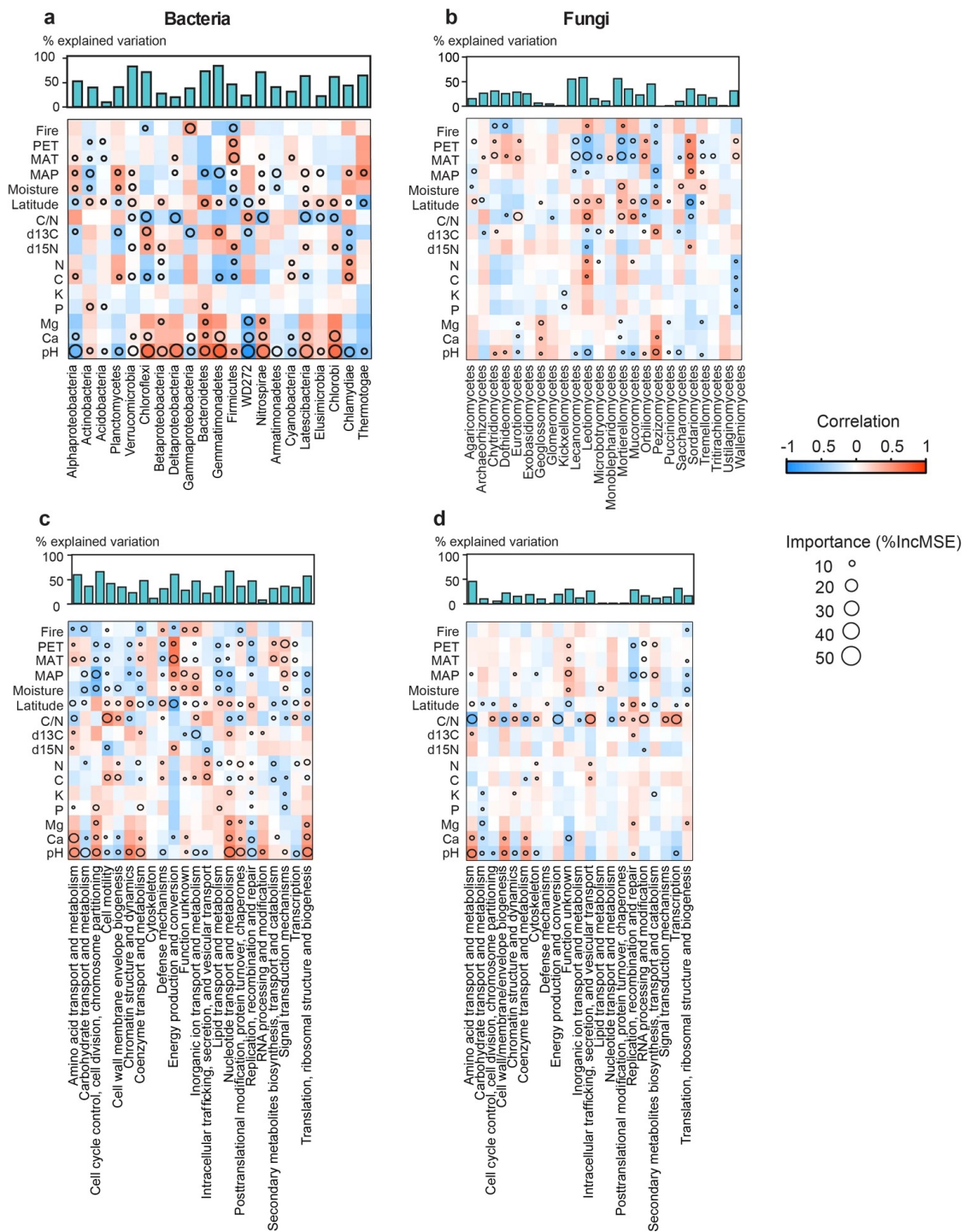




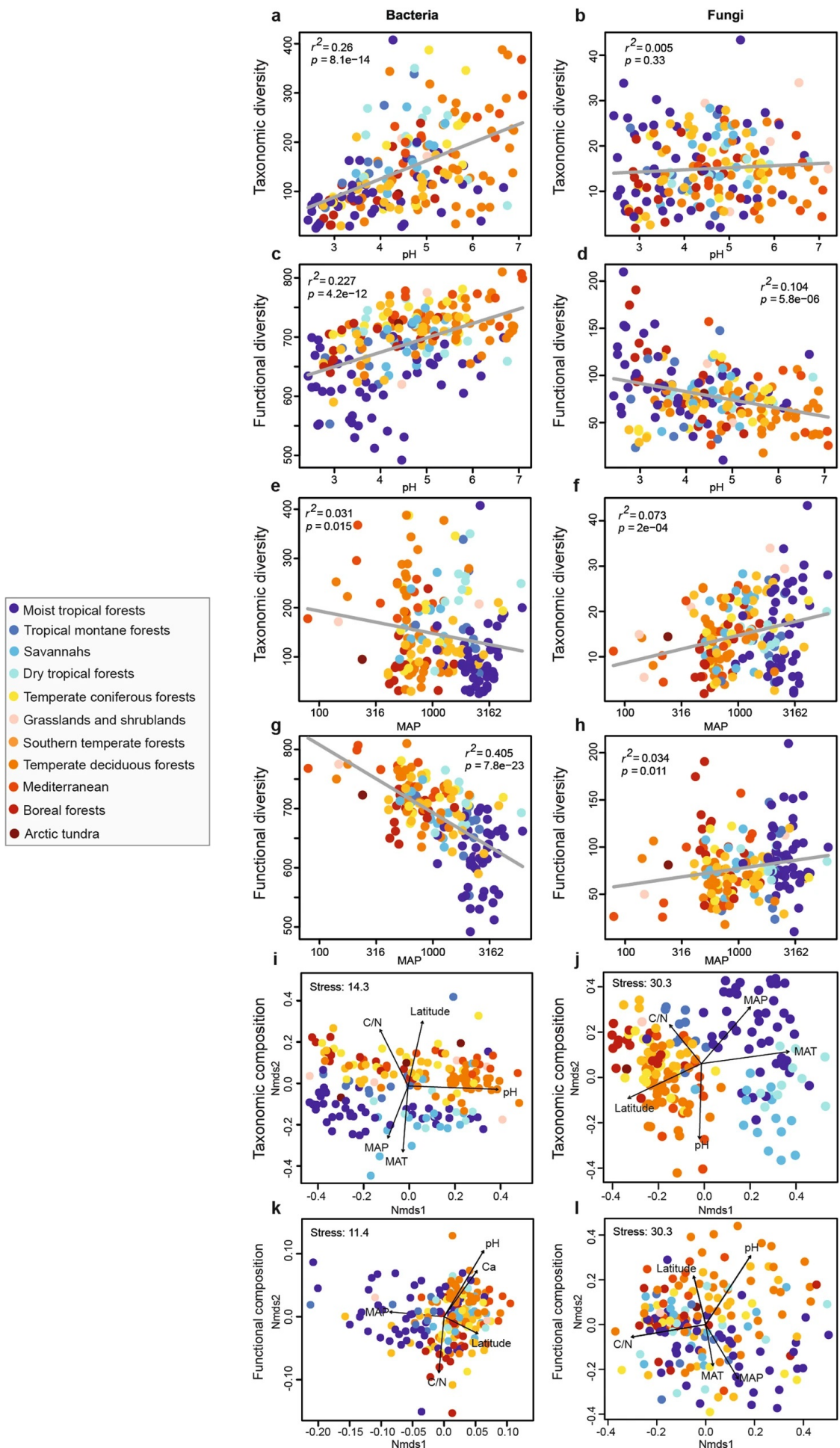
**Extended Data Fig. 3 The significant decrease in the bacterial/fungal biomass ratio with increasing latitude is driven by the joint effect of climate and soil fertility.**



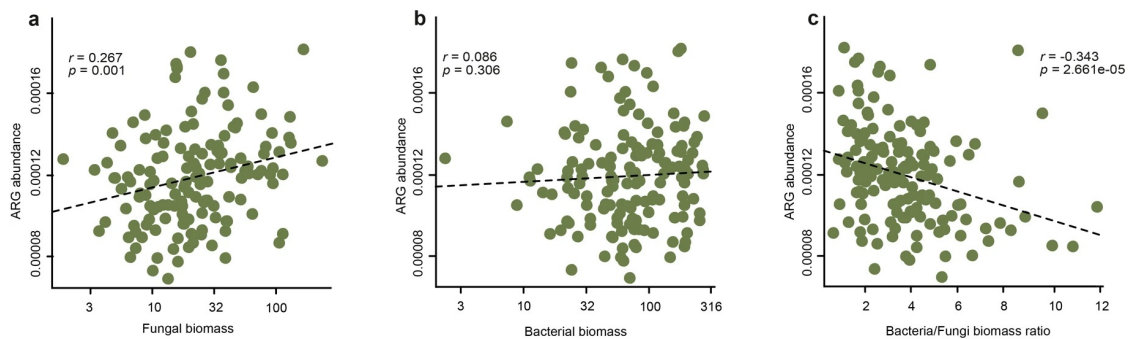
# Extended Data Fig. 4 The environment has a stronger effect on bacterial taxa and functions than those of fungi.



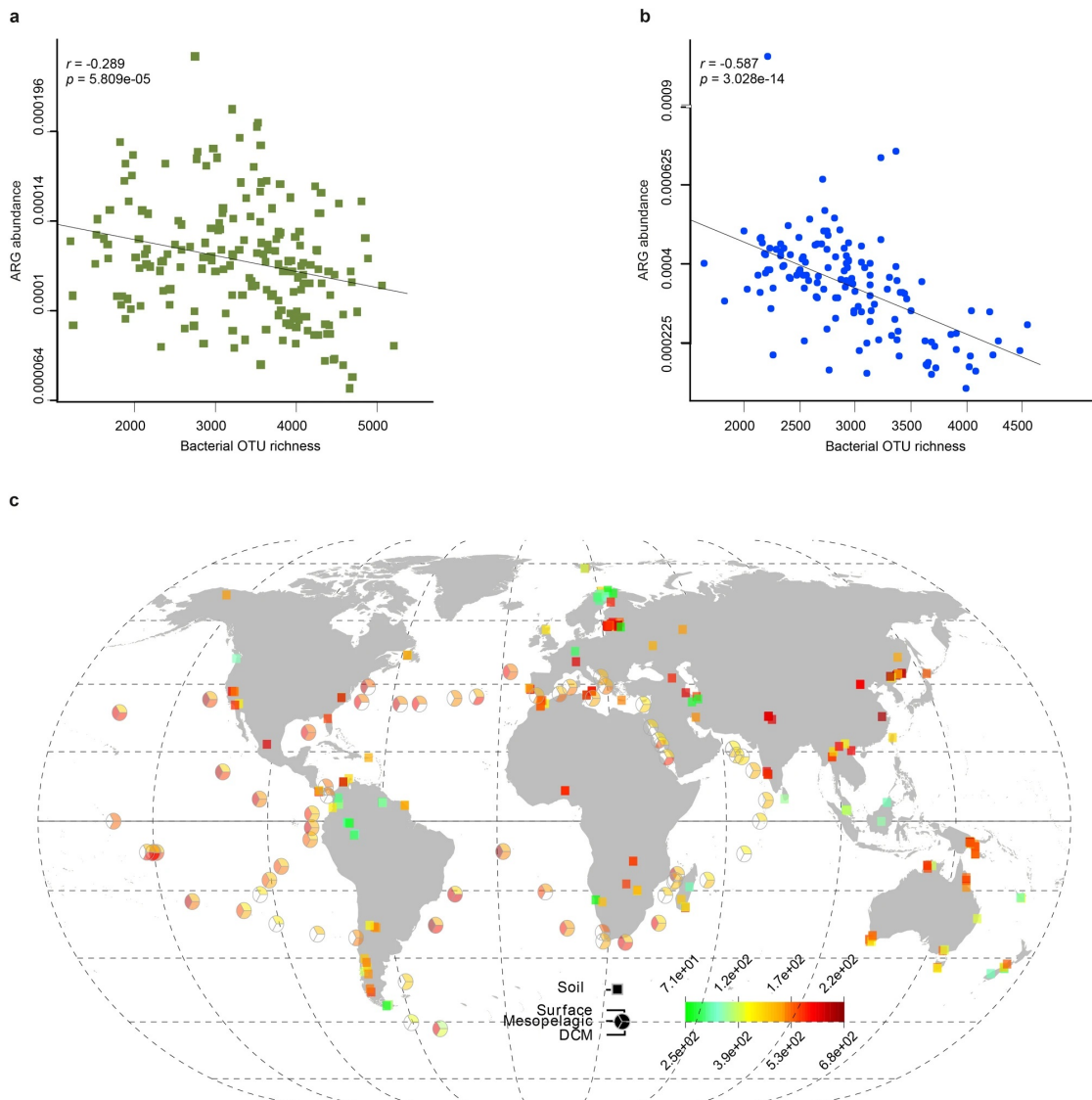
**Extended Data Fig. 5 Niche differentiation between bacteria and fungi is probably related to precipitation and soil pH.**



# Extended Data Fig. 6 Fungal biomass is significantly related to the relative abundance of ARGs.



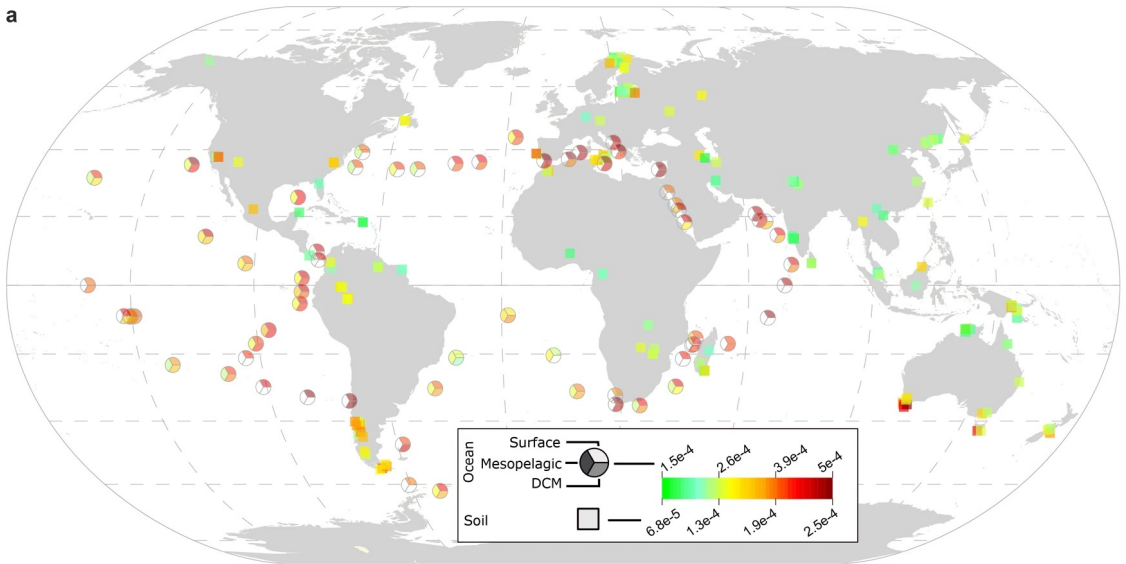
### Extended Data Fig. 7 Topsoil and ocean bacterial phylogenetic diversity is negatively correlated with the abundance of ARGs.



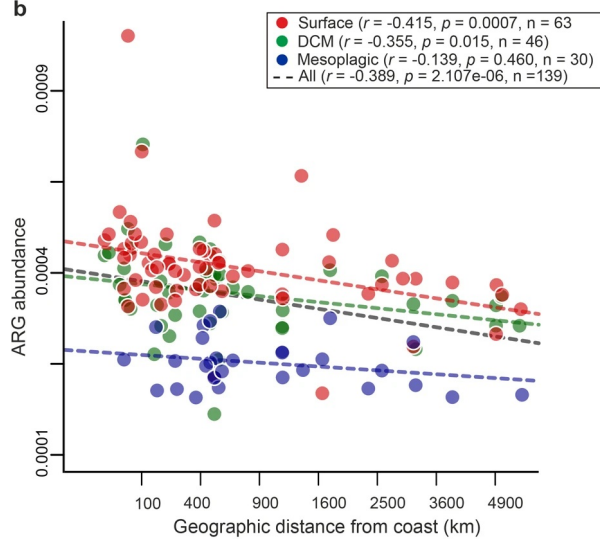


**Extended Data Fig. 8 Relative abundance of ARGs within and between terrestrial and oceanic ecosystems.**

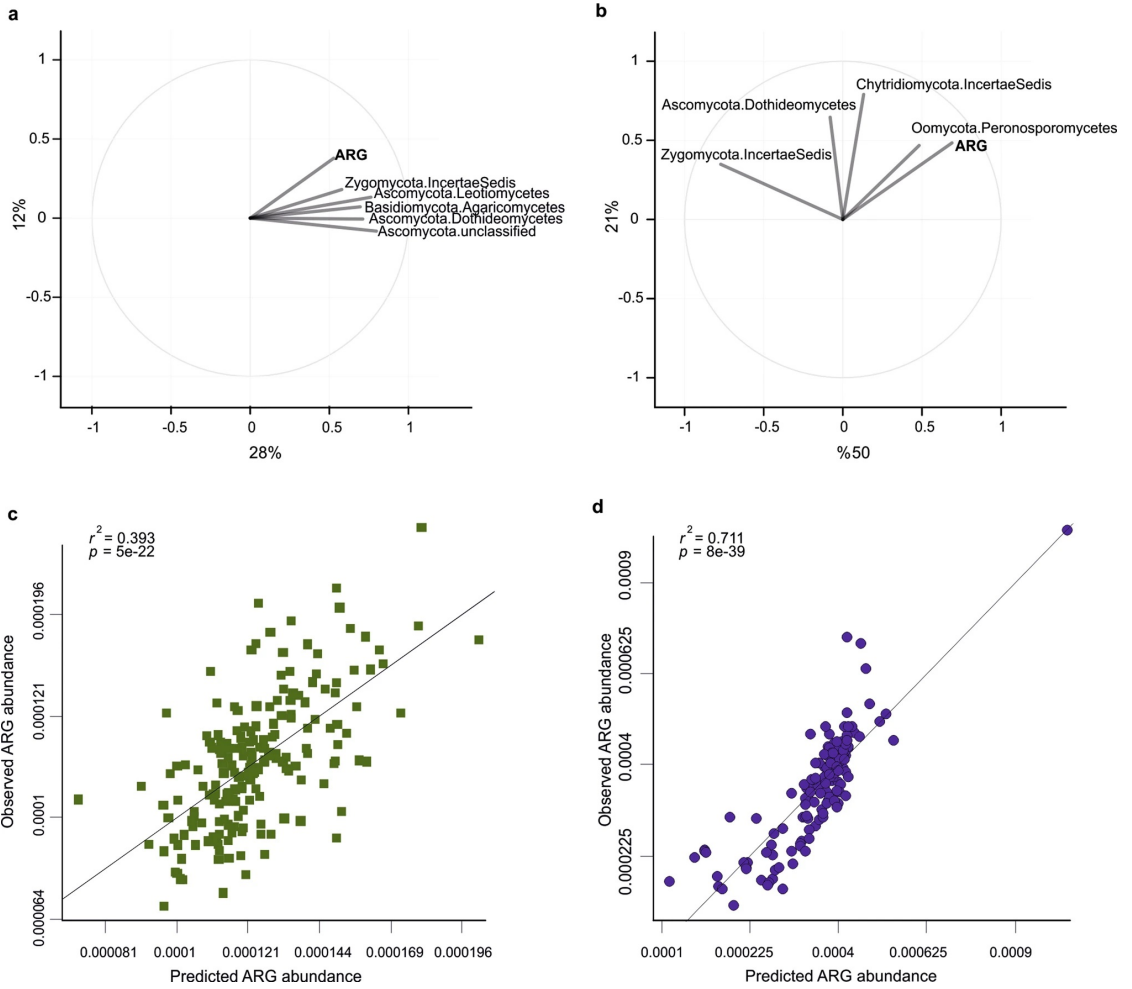
**a**



**b**



**Extended Data Fig. 9 Relative abundance of ARGs in both ocean and topsoil samples can be modelled by the relative abundance of fungi and fungus-like protists.**



# Extended Data Fig. 10 Fungal classes are among the main taxa associated with the relative abundance, diversity and richness of ARGs in different habitats.

